Plasma Assisted Nitrogen Oxide Production from Air: Using Pulsed Powered Gliding Arc Reactor for a Containerized Plant

B. S. Patil[1], F. J. J. Peeters[2], J. A. Medrano[3], G. J. van Rooij[2], F. Gallucci[3], J. Lang[4], Q. Wang[1#], V. Hessel[1] 🆔

[1]Laboratory of Chemical Reactor Engineering / Micro Flow Chemistry and Process Technology, Dept. of Chemical Engineering and Chemistry, Eindhoven University of Technology, P.O. Box 513, 5600 MB Eindhoven, The Netherlands

[2]Dutch Institute for Fundamental Energy Research (DIFFER), P.O. Box 6336, 6500 HH Eindhoven, The Netherlands.

[3]Chemical Process Intensification, Dept. of Chemical Engineering and Chemistry, Eindhoven University of Technology, De Random 70, 5612 AZ Eindhoven, The Netherlands

[4]Innovation Management, Verfahrenstechnik & Engineering, Evonik Industries AG, Rodenbacher Chaussee 4, 63457 Hanau-Wolfgang, Germany.

[#]corresponding authors:

Q. Wang, email: q.wang0207@gmail.com

[1]

Abstract

The production of NO_x from air and air+O_2 is investigated in a pulsed powered milli-scale gliding arc (GA) reactor, aiming at a containerized process for fertilizer production. Influence of feed mixture, flowrate, temperature, and Ar and O_2 content are investigated at varying specific energy input. The findings are correlated with high-speed imaging of the GA dynamics. An O_2 content of 40-48% was optimum, with an enhancement of 11% in NO_x production. Addition of Ar and preheating of the feed resulted in lower NO_x production. Lower flowrates produced higher NO concentrations due to longer residence time in the GA. The volume covered by GA depends strongly on the gas flowrate, emphasizing that the gas flowrate has

a major impact on the GA dynamics and the reaction kinetics. For 0.5 L/min, 1.4 vol% of NO_x concentration was realized, which is promising for a containerized process plant to produce fertilizer in remote locations.

Keywords: milli-scale gliding arc reactor, nitrogen fixation, high speed imaging, pulsed powered, containerized process plant
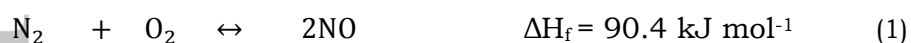
Introduction

The Haber-Bosch process artificially fixes nitrogen to produce ammonia in a centralized production facility to sustain 40% of today's population and numerous other industrial applications, which ought to grow along with the rapidly growing global population.[1,2] However, modern technological and ecological standards demand a considerable reduction in its environmental footprint and an increase in its energy efficiency, as it consumes 1-2% of world's total energy production and emits 300 million metric tons of CO_2.[3,4] Over 160 million tons of ammonia are produced per year[5], therefore even a slight improvement in the process efficiency would yield huge environmental and economic benefits. Thus, it's not a surprise that ammonia has been identified by the International Energy Agency (IEA) as the chemical compound with the highest potential to reduce energy and GHG emissions by 2050 by improving the catalyst and catalytic process[6]. Moreover, changing needs (e.g. localized fertilizer production[7]) and new applications (e.g. electrical energy to chemicals[8]) triggered by a renewable energy generation scenario encourages innovative and sustainable methodologies for chemical nitrogen fixation in the form of NO_x (=$NO+NO_2$) or NH_3.

Among several alternatives, electricity-driven non-equilibrium plasma processes are considered to be very attractive contenders for energy efficient nitrogen fixation.[9,10] It is worth noting that nitrogen fixation via non-thermal plasma (NTP) offers an opportunity to produce fossil-free nitrogen-containing compounds at a considerably lower theoretical energy consumption.[11,12] In NTP, highly energetic electrons collide with bulk gas molecules, yielding a mixture of highly reactive species which enable thermodynamically

unfavorable reactions like nitrogen fixation at atmospheric pressures and lower temperatures.[13,14] Plasma processes are more attractive on smaller scales like in containers or modular plants.[15] Plasma assisted nitrogen fixation on smaller scale will offers an interesting opportunity as atmospheric pressure and ambient temperature processing will substantially improve plant safety and decrease the operational and capital costs compared to the high-pressure Haber-Bosch process.[16] The mild operating conditions and relatively small scale could also encourage development of localized nitrogen fertilizer production plants. The approach of de-centralized chemical production has been undertaken in the EU funded MAPSYN project for plasma assisted nitrogen fixation process[11,12], which would eventually benefit remote places to produce their own fertilizer and fuels, using only renewable energy sources such as solar or wind[17]. Along similar lines, N_2-applied, a Norwegian company, is commercializing the plasma assisted nitrogen fixation process on smaller scale for use by farmers[18].

The overall reactions representing nitrogen fixation with oxygen to give NO_x ($NO + NO_2$), which absorbed in water yield nitric acid, are depicted by reaction 1 and 2. The ratio of NO and NO_2 is determined by the thermodynamic equilibrium and the reaction kinetics[30]. The formation enthalpy of the process (ΔH_f, defined at standard conditions) is fairly high, therefore high temperature are needed to carry out this reaction.

$$N_2 \;+\; O_2 \;\leftrightarrow\; 2NO \qquad\qquad \Delta H_f = 90.4 \text{ kJ mol}^{-1} \qquad (1)$$

$$2NO \;+\; O_2 \;\leftrightarrow\; 2NO_2 \qquad\qquad \Delta H_f = 33.2 \text{ kJ mol}^{-1} \qquad (2)$$

Non-thermal plasma can be effectively realized using Gliding arc reactors, which provide a blend of hot quasi-equilibrium plasma (arc) and cold non-equilibrium plasma (glow), and offers advantages such as atmospheric (or higher) pressure operation, non-equilibrium cold plasma, higher throughput with greater flexibility and also has high selectivity towards chemical reactions[19–22]. Recently, gliding arc reactors have

been increasingly investigated for a range of high throughput plasma processes such as CO_2 conversion to value added products[23,24], CH_4 reforming[25,26], and volatile organic compound abatement[27–29].

Even though the gliding arc reactor offers numerous advantages, it has not yet been thoroughly investigated for NO_x synthesis. Very few studies have been reported on plasma assisted NO_x synthesis in gliding arc reactors[31–34], where the highest concentration of NO_x reported is 7100 ppm[34], although the energy efficiency and concentration of NO_x were not the focal points of these studies[35]. Besides the conventional flat configuration[32,34], gliding arc reactor with 2 and 3 powered electrodes was also investigated using air as a feed[31]. Yang et al. have recently reported NO_x production in a gliding arc reactor operated at high (kHz) and low (Hz) frequency. Gliding arc operation in the kHz frequency range was found to be 3 times more efficient than operation at 50 Hz[36]. In our previous investigation on NO_x synthesis in a milli-scale gliding arc reactor[35], NO_x was produced with relatively higher concentration (9500 ppm) and at an energy efficiency of 28.7 kWh/kg of NO_x. The milli-scale configuration provides an intensified contact between reactive species by minimizing the reactant that bypasses the arc, thus efficiently channelling the applied energy to the reactant gases. This advantage of the milli-scale geometry of the gliding arc reactor led to its exploration for other plasma processes[25,37].

In this investigation, the gliding arc reactor is operated in the kHz-range, yielding roughly 200 more discharges as compared to operation at 50 Hz frequency. This fast, repetitive pulsing is more likely to lead to strong non-equilibrium conditions in the reactor, with electron and vibrational temperatures exceeding the gas temperature ($T_e \approx T_{vib} > T_{gas}$), but also facilitate quenching, obligatory for freezing the NO_x produced, by having a lower gas temperature for a given power input [37]. Moreover, 50 Hz operation provides periods of up to 20 ms in which vibrational excitation of molecules can be lost through vibrational-translational relaxation, this relaxation time is significantly reduced for kHz operation. Therefore, with the approach reported in this study, the significant amounts of internal energy in vibrational modes is expected to be not lost via gas heating, thus leading to more energy efficient chemical conversion.[13]

The possibility to use air instead of pure nitrogen and oxygen is favourable for a containerized process plant from an economic point of view. However, it is unknown how the oxygen percentage would affect the NO_x production and what the optimum oxygen percentage would be. Similarly, the energy consumption per kg of fixed nitrogen is the most important performance parameter, whose dependency on process parameters is often unclear in the literature. Dilution by an inert gas such as argon was found to enhance the amount of nitrogen fixed in a DBD reactor[38], however, its effect is unknown for gliding arc reactors and particularly for NO_x synthesis. By preheating, one can expect to increase the rate of reactions between atomic nitrogen with molecular oxygen to form NO[39]. Furthermore, operation of gliding arc reactor at the standard frequency of 50 Hz has been sufficiently investigated with the application of high speed imaging, but dynamics of the high frequency operated gliding arc reactor is scantily reported in the literature.

Therefore, through this paper, we report a systematic unravel plasma assisted nitric oxide production directly from air at atmospheric pressure and low temperatures in a milli-scale gliding arc reactor, aiming at a containerized process for plasma assisted fertilizer production. Here, we determine the optimum oxygen percentage, including air, air+O_2 and pure N_2 + O_2 feed mixtures, to achieve the highest energy efficiency per kg of nitrogen fixed. We also reveal the dynamics of the milli-scale gliding arc reactor powered with high frequency (kHz) microsecond pulses by employing high speed imaging. The high-speed imaging is combined for the first time with voltage and current signals to identify the development stages of the discharge. Addition of argon and feed gas preheating is also investigated, with the aim of enhancing the NO_x production. Finally, a kinetic scheme of plasma-assisted NO_x synthesis in a gliding arc reactor is postulated.

Experimental

Milli-scale gliding arc reactor and experimental set-up

Plasma NO_x synthesis was performed in a high frequency driven milli-scale gliding arc reactor at atmospheric pressure. A scheme of the experimental set-up is shown in A typical voltage signal (pulse) generated by the waveform generator is presented in Figure SI-1. This square voltage signal is amplified

by the transformer, producing applied voltage signals in the kV range. To achieve the highest NO_x concentration, operational frequency and pulse width of the waveform generator were scanned in the range of 1-40 kHz and 1-30 μs, respectively. The operation of milli-scale gliding arc reactor was found to be optimal at 7 kHz and 25 μs, based on the stability of gliding arc and NO_x concentration. Thus, for all the experiments, waveform voltage signals are introduced to the transformer+reactor system in pulses with a 25 μs duration at a constant repetition frequency of 7 kHz (143 μs). A typical voltage-current signal for milli-scale gliding arc reactor operation is shown in Figure 2. A waveform voltage of 60 V_{pk-pk} was chosen for this figure, as it very clearly shows the transitions between different discharge regimes, as will be discussed in the results section. The experiments of O_2 %, argon dilution and feed gas preheating were performed at a constant waveform generator voltage of 44 V_{pk-pk}, translating to a high voltage on the electrode of up to 6 kV. Operating at this lowest waveform generator input voltage guaranteed uniform experimental conditions without excessive heating of the reactor, unlike reactor operation at higher input voltage (which has corresponding higher applied voltage). Power consumption was obtained by averaging over at least 100 cycles. The temperature of the outlet gas was monitored with a thermocouple installed at the exit of the reactor. Maximum outgoing bulk gas temperature was found to be 313 K.

Figure 1. The gliding arc reactor is of Macor® with quartz glass cover on top for visual observations. The reactor consists of two thin diverging knife-shaped tungsten electrodes with thickness of 2.5 mm and height of 80 mm. The width of the reactor is 50 mm with the narrowest point between electrodes being 2 mm. One of the electrodes is connected to the high voltage source and another electrode is grounded. The reactor was powered by a customized Xenionik EP 4000 AC power supply + transformer system, operated via a waveform generator. High voltage (kV) was measured with Tektronix P6015A probe. Current (I_{GA}) flowing through the gliding arc was measured by using the resistor method, where voltage (V_R) was measured across a resistor (R = 5 Ω). Calculation for the energy input per pulse (E) to the plasma reactor, total power, specific energy input (SEI), and the energy consumption per mole of NO_x are defined by Eq. 3-7, respectively.

$$I_{GA} = \frac{V_R}{R} \tag{3}$$

$$E = \int_{t=0}^{t=t_{pulse}} (I_{GA} * V) dt \tag{4}$$

$$\text{Total Power} = E * f \tag{5}$$

$$\text{Specific Energy Input (SEI)} = \frac{\text{Total Power} \left(\frac{J}{s}\right)}{\text{Gas Flowrate} \left(\frac{L}{s}\right)} \tag{6}$$

$$\text{Energy consumption per mole of NO}_x = \frac{\text{Total Power} \left(\frac{J}{s}\right)}{\text{Mole of NO}_x \text{ produced} \left(\frac{mol}{s}\right)}, \tag{7}$$

where t_{pulse} is the time span of a pulse (s), f - frequency (Hz), and the energy efficiency is defined to be the reciprocal of energy consumption per kg mol of NO_x.

A typical voltage signal (pulse) generated by the waveform generator is presented in Figure SI-1. This square voltage signal is amplified by the transformer, producing applied voltage signals in the kV range. To achieve the highest NO_x concentration, operational frequency and pulse width of the waveform generator were scanned in the range of 1-40 kHz and 1-30 μs, respectively. The operation of milli-scale gliding arc reactor was found to be optimal at 7 kHz and 25 μs, based on the stability of gliding arc and NO_x concentration. Thus, for all the experiments, waveform voltage signals are introduced to the transformer+reactor system in pulses with a 25 μs duration at a constant repetition frequency of 7 kHz (143 μs). A typical voltage-current signal for milli-scale gliding arc reactor operation is shown in Figure 2. A waveform voltage of 60 V_{pk-pk} was chosen for this figure, as it very clearly shows the transitions between different discharge regimes, as will be discussed in the results section. The experiments of O_2 %, argon dilution and feed gas preheating were performed at a constant waveform generator voltage of 44 V_{pk-pk}, translating to a high voltage on the electrode of up to 6 kV. Operating at this lowest waveform generator input voltage guaranteed uniform experimental conditions without excessive heating of the reactor, unlike reactor operation at higher input voltage (which has corresponding higher applied voltage). Power consumption was obtained by averaging over at least 100 cycles. The temperature of the outlet gas was monitored with a thermocouple installed at the exit of the reactor. Maximum outgoing bulk gas temperature was found to be 313 K.

Figure 1. Schematic of the milli-scale gliding arc and the experimental set-up.

Flowrates of N_2, O_2 (Linde Gases, 99.9%) and dehumidified air were controlled using mass flow controllers (Bronkhorst). The reaction products were analysed inline using a Fourier Transform Infrared Spectrophotometer (SHIMADZU, IRTracer-100) at resolution of 0.5 cm^{-1} with the gas cell equipped with CaF_2 windows (Specac). NO and NO_2 were the only products detected, their concentrations determined from the adsorption bands at 1900 cm^{-1} and 1630 cm^{-1}, respectively, using a series of calibration gas mixtures. All the experiments were performed twice and reproducibility of NO_x concentration was found to be within ± 5 %. All graphs involving concentrations therefore show an estimated 95 % confidence interval bar. The concentration of NO_x was determined as a sum of NO and NO_2 concentrations. Hence, reported NO selectivity was calculated using Eq. 8:

$$\text{Selectivity of NO} = \frac{\text{Concentration of NO}}{\text{Concentration of (NO+NO}_2)} \qquad (8)$$

High-speed recordings

Images of the gliding arc propagation have been taken using a CMOS high-speed camera (HighSpeedStar 5.1) which allows a maximum frame rate of 3.6 kHz at maximum resolution of 1024 by 1024 pixels (and up to 500 kHz at lower resolutions). Prior to the recordings, optimization of the imaging conditions was performed by changing the frame rate and exposure time of the detector in order to allow the visualization of the propagation of the gliding arc. A set of experiments at different frame rates have been designed in order to better understand the formation and life-time of the gliding arcs operating at a fixed pulsing frequency of 7 kHz for different inlet gas flow rates (1.0, 0.7, and 0.5 L/min) (refer to the supplementary information Table SI-1 for experimental details). For the recordings, a camera exposure time of 40 μs has been selected based on the superior detection of the arcs, within the duration of a single high voltage cycle. The image intensity of the gliding arc has been further enhanced by subtraction of a background image corresponding to the reactor without plasma. Post-processing of the images has been performed using the commercial software Davis 8.0 from LaVision. Average gliding arc height (mm), average gliding arc propagation time (ms) and the average gliding arc velocity (m/s) have been

evaluated for different experiments as tabulated in the Table SI-1. Average gliding arc height is the maximum height to which discharging can propagate, as measured from the narrowest point between the electrodes. Gliding arc propagation time is defined as the time needed for consecutive arcs to move from the narrowest point between the electrodes to the average gliding arc height. Average gliding arc velocity is the ratio of average GA height and GA propagation time. High-speed imaging allows arc tracking by the displacement of the arc position every 0.04-0.06 ms (depending on the experiment reported in table SI-1). Therefore, the arc velocity is experimentally measured by the displacement of the arc in the central position of the reactor. Furthermore, since every arc propagation, cycle can be visualized (see attached media file), the average time between first arc ignition (at the narrowest point) and final arc dissipation (at the maximum height) is also measured. The analysis and discussion of the high-speed recordings is presented in the following section.

Figure 2. Voltage-current signal for the milli-scale gliding arc reactor with different scope resolutions (a) A complete gliding arc cycle of ~8 ms duration (b) Ignition of arc with currents up to ~25 A, (c) Propagation of arc with current < 1 A (at 7 kHz-25 μs, 0.5 L/min of Air+O_2 with N_2/O_2 ratio=1 and waveform generator input voltage 60 V_{pk-pk}).

Results and discussion

High speed imaging of arc development

Image analysis of the experiments has been performed with two different objectives: i) to deduce the arc dynamics such as average velocity of the gliding arc, lifetime of a gliding arc and its relationship with gas flow velocity and ii) to establish the relationship between gliding arc propagation and the voltage-current signal.

A real time development of the gliding arc can be viewed from the **attached media file**. First, it is observed that only one arc can form in the reactor at any time, as already observed in literature by other authors for gliding arcs[41]. Any arc that forms will necessarily be extinguished whenever the applied voltage drops below some critical value, which at the applied voltage frequencies used in this work will

occur within ~ 100 μs of ignition. This can be observed in the voltage-current signals depicted in Figure 2a-c. The high speed imaging reveals how repeated ignitions every cycle of the applied voltage lead to a propagating behaviour of gliding arcs. Propagation as a function of time is depicted in Figure 3. Ignition of an arc at the narrowest point is observed in Figure 3a, with subsequent ignitions occurring at increasingly higher points in Figure 3b-f over a period much longer than the duration of an applied voltage cycle.

Table 1. Summary of the Results obtained by High Speed Imaging

Average gliding arc height (mm), average gliding arc propagation time (ms) and the average gliding arc velocity (m/s) have been evaluated for different conditions and are listed in Table 1. Comparing the average gliding arc propagation time (max. 14.5 ms) to the duration of a single applied voltage cycle (143 μs), it is seen that propagation consists of up to 101 arc re-ignitions. In order to compare these numbers to the gas flow rate, the following expression is used to calculate the average gas flow velocity $<v_{gas}>$ within the reactor volume exposed to arcs:

$$\langle v_{gas} \rangle = \frac{\Phi}{\delta} \left(\frac{1}{w_0 + \Delta x \cot \alpha} \right), \tag{9}$$

with Δx the average gliding arc height, δ the thickness of the electrodes (2.5 mm), w_0 the gap width at the narrowest point (2 mm), Φ is the gas flow rate and α is the angle of the electrodes with the horizontal (80°). The derivation of Eq. (9) is provided in the Supplementary Information (SI-3). The results of Eq. (9) are shown in the last column of Table 1. Comparing these numbers to the average gliding arc velocity, it is seen that they are very similar, but with average gas flow velocity at least 22% higher than average arc velocity. This discrepancy is assumed to be due to measurement error and it is concluded that arc re-ignition follows the gas flow. The arc re-ignites at higher and higher points every cycle because the gas flow carries with it sufficient residual electrons and ions from the previous (half-)cycle to reduce the breakdown voltage and allow for preferred ignition at wider gap widths. After a critical height is reached, at which the applied voltage is no longer sufficient to re-ignite an arc, re-ignition once again occurs at the narrowest point between the electrodes. As can be noticed from Table

1, lower feed flow rate leads to a higher gliding arc propagation time and slower gliding arc velocities. This is because higher flowrates force arcs to move upwards faster. However, these faster arcs become more elongated, with a more uneven symmetry from the centre of the reactor. With total arc length disproportionally increased compared to arcs with lower flowrates at the same height, extinction of the arc will occur sooner as the required electric field (the ratio of applied voltage and arc length) for re-ignition cannot be supplied. The rising of the arc through the reactor was found to be asymmetric, since the arc moves faster at the high voltage electrode than at the grounded electrode, as can be seen in Figure 3. Similar phenomena have been observed by Tu et al.[42] This can potentially be caused by a non-uniform velocity field of the feed gas. It is important to note that as consecutive arcs travel up the reactor, the volume of gas trailing below it never has plasma ignited in it. The size of this 'trailing volume' of gas depends on the time between re-ignitions at the lowermost point.

Comparing the fast imaging results with V-I signals (Figure 2), the ignition of an arc at the narrowest point occurs at the highest applied voltage with high current, short duration pulses ($\sim$25 A, see Figure 2b). After ignition, both applied voltage and current drop instantaneously within a few nanoseconds. Once the first arc is ignited, the voltage required to re-ignite it in following applied voltage cycles decreases from 6 kV to $\sim$2.5 kV. After the first $\sim$10 re-ignitions, the arc develops into prolonged discharges with low current ($\sim$100 mA) and durations of $\sim$50 μs (see Figure 2c). These prolonged discharges contribute significantly to the power consumption. The average impedance of the arc increases from $\sim$ 250 Ω for the very first ignition to $\sim$ 10 kΩ for the prolonged discharges. This increase points to a much lower electron density in the arcs igniting higher up the reactor, which is an indication of non-equilibrium discharging, since the electron temperature must increase to sustain the arc. The initial, short duration, high-current arcs are likely thermal, with equal electron temperature T_e, vibrational temperature T_{vib} and gas temperature T_{gas}, while the increase in T_e higher up the arc will likely lead to increased vibrational excitation, providing $T_e > T_{vib} > T_{gas}$[43].

Figure 3. Visualization of the gliding arc propagation along the reactor as a function of time by means of high speed recordings for the inlet feed flow rate = 1 L/min; N_2/O_2 = 1. Frame rate = 3 kHz with resolution of 512 X 512.

Effect of feed and O_2 %

The production of NO_x is investigated by employing different feed options (air, air+O_2 and N_2+O_2) and with varying O_2% in the feed at 7 kHz, 25 µs and keeping the amplitude of input voltage constant at 44 V_{pk-pk}. The percentage of oxygen in the feed gas has a strong impact on the amount of NO_x produced and the NO selectivity as shown in Figure 4a and 4b respectively. Small fractions of gas impurities present in air, such as Ar (< 1%) and helium, could influence plasma discharge properties and affect the production of NO_x. However, the feed used, either air or N_2+O_2, does not influence the concentration of NO_x produced as long as the percentage of N_2 and O_2 are similar in the feed gas (Figure 4a). These results give a clear indication that air can also be used as a feed instead of pure N_2 and O_2 for plasma NO_x synthesis. Therefore, for containerized plasma NO_x production units, only air filter/ dehumidifier will be needed, thus saving operating and investment cost associated with air separation in pressure swing adsorption unit. Moreover, the NO_x concentration decreased slightly when only air is used, without adding extra oxygen. The decrease is 24 % for 1 L/min and ~18 % for 0.7 and 0.5 L/min (comparing NO_x concentrations obtained at 20% and 40% O_2 in Figure 4a). The concentration of NO_x for air+O_2 and N_2+O_2 passes through a maxima, irrespective of the flowrate. Air with 35 to 48 % oxygen seems to be an optimum feed composition. Above 48% oxygen, overall NO_x concentration steadily declined. Specific energy input slightly increases when feed gas has more than 48% oxygen. As shown in SI-4 (Figure SI 2), the increase is around 6% for 1 L/min and 4% for 0.5 L/min.

Figure 4b shows the effect of the O_2 percentage on the NO selectivity (defined by Eq. 8). NO selectivity decreases linearly with increasing O_2 percentage till 48%, after that NO selectivity is constant.

Figure 4. Effect of different feeds and N_2/O_2 ratio on- a. NOx concentration and b. NO selectivity (frequency= 7 kHz, input power ~ 12 W with SEI between $700 - 1500$ J/L).

For NO selectivity in the exhaust of the gliding arc reactor, the following reaction is the most relevant:

$$NO \ + \ NO \ + \ O_2 \ \leftrightarrow \ NO_2 \ + \ NO_2 \qquad\qquad (10)$$
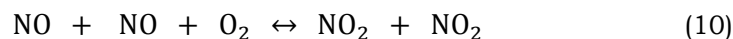
Reaction 10 is highly sensitive to temperature. Figure 5 shows the selectivity towards NO as predicted by reaction 10 for different oxygen content and gas temperatures. Comparing this to the experimental results in Figure 4, the observed NO selectivity can be accounted for if the gas is still at elevated temperatures during the measurements, or if the mixture has not yet attained full equilibrium. At 300 K, the forward reaction rate of reaction (10) is 10^{-50} m^6s^{-1}, dropping to 10^{-51} m^6s^{-1} at 600 K. Combined with an NO concentration of 4000 ppm and an O_2 concentration of $1.2 \cdot 10^{25}$ m^{-3} (50 % O_2), a lifetime of NO at 300 K of ~ 50 s is found and ~ 500 s at 600 K. The time for gas species from the plasma to reach the FTIR cell is approximately $2 - 10$ s, depending on flow rate. There is, therefore, insufficient time for the NO/NO_2 concentration to equilibrate to room temperature values (i.e. 0% NO selectivity via Figure 5). The observed selectivity in Figure 4b is, therefore, a signature of the composition within the reactor, which matches more closely to a gas temperature of ~ 450 - 475 K.

In the gliding arc reactor, the temperature is very high in the arc core, with the afterglow at intermediate temperatures between hot core and ambient temperature. Assuming all the power goes to gas heating, an upper limit on the maximum average temperature T_{gas}^{max} in the reactor can be determined:

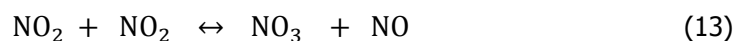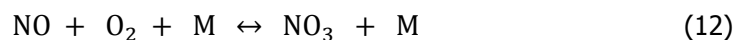$$T_{gas}^{max} = T_0 + SEI/C_p \qquad\qquad (11)$$

with T_0 the ambient temperature, SEI the specific energy input in J/L and C_p the specific heat capacity of the gas mixture at constant pressure expressed in J/LK which is 1.28 J/LK for air (which is a good estimate for other $N_2 + O_2$ mixtures as well). For the data in Figure 4, assuming no energy goes into reactions, maximum average gas temperatures of 820 K (flow rate 1 L/min = ~700 J/L) and 1450 K (flow

rate 0.5 L/min = ~1500 J/L) are found. A detailed analysis of kinetics in the arc core and surrounding afterglow are addressed in our recent publication[43].
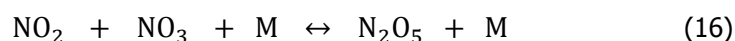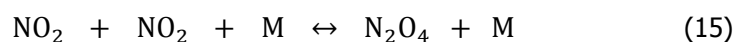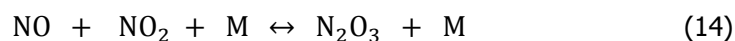
Figure 5. NO selectivity at equilibrium for different oxygen content as a function of gas temperature. The solid line is for 50% O_2 content and the dashed lines for 20% and 80%.

Production of other N_xO_y species

The data in Figure 4 can be used to quantify nitrogen oxides not observed in FTIR. The species to be considered are NO_3, N_2O_3, N_2O_4 and N_2O_5. For NO_3, the main reactions affecting its concentration at room temperature are:

$$NO + O_2 + M \leftrightarrow NO_3 + M \qquad (12)$$

$$NO_2 + NO_2 \leftrightarrow NO_3 + NO \qquad (13)$$

For the N_2O_y species these are:

$$NO + NO_2 + M \leftrightarrow N_2O_3 + M \qquad (14)$$

$$NO_2 + NO_2 + M \leftrightarrow N_2O_4 + M \qquad (15)$$

$$NO_2 + NO_3 + M \leftrightarrow N_2O_5 + M \qquad (16)$$

For reactions 12 – 16, forward and backward reaction rates are shown in Table 2. In the same table, the concentrations of NO_3, N_2O_3, N_2O_4 and N_2O_5 are estimated for 450 K from the measured maximum concentrations of NO and NO_2 in Figure 4, i.e. [NO] ≈ 4000 ppm and [NO_2] ≈ 3000 ppm at 50% oxygen content and a flow rate of 0.5 L/min. From the slow forward rates for reactions 12 and 13, it is obvious

that NO_3 is highly unstable and its concentration can be neglected. The same is therefore also true for N_2O_5 via reaction 16. The concentrations of N_2O_3 and N_2O_4 are slightly more significant, though still in the parts per billion range and thus negligible compared to those of NO and NO_2. The forward rates in Table 2 go down further with increasing gas temperature, while the backwards rates go up, implying that in the much hotter plasma, the concentrations of higher nitrogen oxide species are even lower[39].

Table 2. Rates for Production and Destruction of Higher Nitrogen Oxides at 450 K [39]

Effect of flowrate

To investigate the influence of the flowrate, three different feed gas mixtures were prepared, in particular a $N_2 + O_2$ mixture (N_2/O_2 ratio = 1), Air (N_2/O_2 ratio ~ 4) and Air + O_2 (to have N_2/O_2 ratio = 1). Note that the difference between $N_2 + O_2$ and air + O_2, with the latter containing trace impurities, is also investigated in the section on O_2 %, but is here included with a constant N_2/O_2 ratio only. During these experiments, NO_x concentration was measured with increasing specific energy input (SEI) for three different flowrates; 1.0 L/min, 0.7 L/min and 0.5 L/min. Experimentally, it has been found that the NO_x concentration increases linearly with the input SEI for all flowrates, as shown in Figure 6a (and Figure SI-3). Table 1 shows the gliding arc propagation time for flow rates between 0.5 – 1.0 L/min, related to SEI between 1450 – 700 J/L. For higher SEI (lower flow rates), the residence time of the gas in the plasma is increased, from 4.2 ms (700 J/L) to 14.5 ms (1450 J/L). At the same time, the average width of the arc channel barely changes with SEI, for 1450 J/L this is found to be 3.8 mm versus 3.2 mm at a SEI of 700 J/L (see SI-3 for the relevant equation). Thus, the contact time with arc discharges on their way through the reactor is the determining factor in conversion to NO_x. Air (N_2/O_2 ratio ~4) was found to consume marginally lower energy than N_2-O_2 and oxygen rich air mixture (both N_2/O_2 ratio =1), when compared at the same flowrate, however it also produces less amount of NO_x than N_2-O_2 mixture. The highest concentration of NO_x, 1.4 vol%, was obtained for 0.5 L/min at expense of 4.7 kJ/L of energy.

Figure 6. Effect of flowrate on- a. NO$_x$ concentration and b. NO selectivity (at frequency= 7 kHz, input power between 12 – 40 W).

The NO selectivity for different flowrates and feed mixtures is shown in Figure 6b. All flowrates show a linear decrease in the NO selectivity with respect to increasing SEI, likely because the longer contact time with plasma at these conditions increases reactions of NO with activated oxygen species to form NO$_2$. Feed mixtures with higher oxygen content tend to have lower NO selectivity as discussed in the previous section. Air+O$_2$ mixtures produced higher amounts of NO$_2$ as compared to only air, e.g. the selectivity for NO in case of air+O$_2$ was decreased by 79% for 0.7 L/min as compared to only air. The oxygen rich, Air+O$_2$ has on an average 40% lower NO selectivity as compared to only air. The 0.5 L/min flowrate produced higher percentages of NO$_2$ than 1 L/min flow, which is due to the increase in the effective residence time of gas species and also the higher energy input per unit volume. These two effects give adequate time and ample reactive species, respectively, for reaction 2 to take place. To produce the desired product, either NO or NO$_2$, the process conditions can be tuned accordingly. For example, to achieve higher concentrations of NO, only Air must be fed and operated at lower range of SEI. To achieve higher amounts of NO$_2$, air+O$_2$ must be fed and the reactor must be operated in higher range of SEI.

Effect of argon addition

Indarto et al.[44] reported an improved conversion of methane and higher hydrogen selectivity when argon and helium were added in the feed gas. Studies in a DBD reactor by Hong et al. found a positive effect of argon addition on the production of ammonia[38], increasing conversion of hydrogen to NH$_3$ from 1.7% to 4.2 %. Thus, feed gas was diluted with argon, with an expectation of achieving higher nitrogen-oxygen conversion and NO$_x$ concentrations.

The feed gases, air and air + oxygen (with N$_2$/O$_2$=1) were diluted with 1.5 to 5 % argon, and the total flowrate was kept constant at 1 L/min. As can be seen from Figure 7a, however the argon addition was found to have a negative impact on the NO$_x$ production, since the concentration of NO$_x$ decreased with increasing argon dilution percentage for both air and air + oxygen. Argon addition is found to decrease

the concentration of the NO_x formed by 5% and 10% for air+O_2 (with N_2/O_2=1) and air, respectively. Because the ionization energies of argon and nitrogen are of a similar magnitude, it can be expected that the plasma is unaffected by the presence of argon, i.e. the degree of ionization will remain the same. With equal degree of ionization, it can also be expected that electron temperature will remain the same at equal SEI, independent of the amount of argon. This further implies that electron-neutral interaction remains the same and the only effect of argon addition is on the neutral-neutral chemistry occurring subsequent to the discharges. In both cases, it can be assumed that a 5% dilution with Ar simply leads to a 5% dilution of the reaction products, without a significant effect on the reaction chemistry. The increase in argon concentration does, however, lead to a ~ (5 ± 3) % decrease in the energy input to the plasma (see also Figure SI-4), due to lowered breakdown voltage in the presence of argon. This also changes the magnitude of the electric field along the arc compared to nitrogen and oxygen. This reduction in electric field (and SEI) can be expected to lead to a decrease in the electron temperature, reducing the production of NO_x. Any further changes to the NO_x formation may be attributed to the changes in residence time of the gas within the arc discharges, since the gliding arc was found to become weaker (attaining a lower Δx) with addition of argon and at higher argon concentrations gliding of the arc was completely absent ($\Delta x \sim 0$). The significant increase in ammonia yield with addition of Ar observed by Hong et al. may be due to reactor type (DBD versus gliding arc) or the presence of catalytic surfaces in their case[38].

Figure 7b shows the effect of argon dilution on the NO selectivity. Selectivity for NO is found to increase with increasing argon dilution by 8% and 2.5% for air and air+O_2 respectively. Increase in argon percentage in the feed diminishes the available oxygen species, thereby slightly reducing NO oxidation to NO_2.

Figure 7. Effect of Ar addition on- a. NO_x concentration and b. NO selectivity (at frequency= 7 kHz, power input ~ 12 - 10 W).

Influence of feed gas preheating

Preheating of the reactor feed is a commonly adapted approach in process industry to recover the heat produced in the reactor, which helps in improving the energy efficiency of the process. Similarly, the heat generated in the gliding arc reactor due to heating of the electrodes can be recovered to heat the feed mixture. The effect of preheating of the feed mixture on the gliding arc discharge behaviour is unknown. Therefore, as a first step, the feed mixture is heated to different temperatures by external electrical heating and the performance of the reactor in terms of NO_x concentration is investigated.

By preheating the feed mixture, additional internal/rotational energy will be supplied, which i) increases the probability in overcoming activation energies and ii) decreases gas density, allowing for longer mean free paths of electrons with a possible increase in electron energy. This last could lead to increased vibrational excitation, which leads to higher NO_x formation rates and a possible decrease in the energy consumption[13]. The feed gas, air and air + oxygen ($N_2/O_2=1$), was heated from room temperature to 473 K using electric heating (up to 5 W) while the total flowrate was kept constant at 1 L/min. As previously calculated using Eq. (11), the maximum *average* gas temperature in the reactor could be as high as 820 − 1450 K, with preheating adding an additional 180 K (473 K − 298 K). Considering that the power is actually deposited in thin arcs, the local gas temperature in the plasma is likely to be even higher. The level of pre-heating is therefore expected to increase plasma gas temperatures by < 10%, which should nonetheless be sufficient to observe its effects. As can be seen from Figure 8, preheating of the feed gas has a negative impact on the amount of NO_x produced. Concentration of NO_x was found to decrease by ~30% at higher temperature as compared to ambient temperature operation. When temperature of the feed mixture is increased from 298 K to 473 K, the initial density of the feed mixture will decrease by a factor of 0.6, giving rise to higher gas flow velocities, which in turn reduces the residence time of the reactants in the plasma. This will lead to less NO_x formation, as was argued in the section on flowrate.

The gliding discharge was also observed to get weaker in terms of dissipated power with increasing temperature. The SEI was found to decrease by ∼ 15% with the increase in temperature (Figure SI-5), with equal settings of the generator circuit. This can also be attributed to the decrease in the gas density.

From Ohm's law: $P = V^2/R$, a lower power dissipation at the same voltage implies a higher resistivity. This could indicate a lower ionization degree at higher temperatures, which could be explained by the slight decrease in gas density: longer mean free paths for electrons leading to fewer electron impact ionization reactions. Lower electron density may lead to higher electron temperatures, as well. At higher electron temperature, more electron impact of N_2 might occur, leading to increased vibrational excitation and dissociation, which in turn leads to an increase in NO_x formation. This could explain why the curve in Fig 7 levels off at T > 400 K. The reduction in electrons is then offset by an increase in electron temperature.

Figure 8. Feed gas preheating has negative impact on NO_x concentration (at frequency= 7 kHz, input power between 12 W plasma + 0 W electric heating (lowest temperature) and 10 W + 5 W electric heating (highest temperature)).

Energy efficiency for plasma NO_x synthesis

Figure 9 shows the energy efficiency for atmospheric pressure plasma NO_x synthesis in the milli-scale gliding arc reactor for various feed mixtures, O_2 % and flow rates. Energy required per mol of NO_x produced has a parabolic trend for all the feed mixtures, O_2 % and flowrates investigated, reaching minima in energy required and then increasing again, as shown in Figure 9a and Figure 9b. For O_2 % (Figure 9a), the lowest energy consumption is obtained at an oxygen content of 40-48%, which corresponds to an N_2/O_2 feed ratio of ~1. Also from Figure 9a, the effect of flow rate on energy efficiency is minimal, though Figure 9b shows that flow rate does affect the amount of NO_x produced.

Figure 9. Energy efficiency of Plasma NO_x synthesis- a. for different O_2 % in feed and b. for different flowrates. (Plasma power between 12 − 44 W).

The lower the flow rate, the higher the exposure to arc discharges, as was revealed by fast imaging. Clearly, it is this longer exposure to arcs which results in greater conversion to NO_x. The energy efficiency will, however, decline as additional arcs contribute less and less to NO formation and more of the power is wasted in the form of heat. Similarly, too little, or too much O_2, will shift the balance of NO formation efficiency away from the optimum.

Among all, vibrational excitation is reported as the most energy efficient channel for nitric oxide synthesis in non-thermal plasma[13], a process mediated by the electrons in the plasma:

$$N_2(v = 0) + e \leftrightarrow N_2(v > 0) + e \tag{17}$$
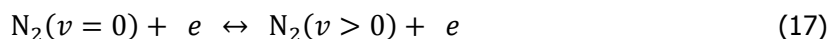
Vibrational excitation drives the so-called Zeldovich mechanism:

$$N_2(v > 0) + O \leftrightarrow NO + N \tag{18}$$

$$N + O_2 \leftrightarrow NO + O \tag{19}$$

It is shown by our recently published work on 0D modelling that vibrational excitation of nitrogen following a so-called Zeldovich mechanism is the most dominant channel for the NO_x formation in a gliding arc reactor[43].

The main undesirable reaction, leading to lower conversion efficiency is the recombination of NO with atomic N, i.e. the reverse reaction of (18). NO_2 is also efficiently consumed in the following back reaction:

$$N + NO_2 \leftrightarrow N_2 + O_2 \tag{20}$$

The main channel responsible for the initial formation of atomic O is electron impact dissociation:

$$O_2 + e \leftrightarrow O + O + e \tag{21}$$
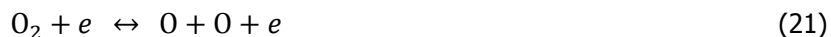
Sufficient O_2 must be present to optimize the Zeldovich chain reactions of (18) and (19), which as shown in Figure 9a, is at $N_2/O_2 = 1$, matching the stoichiometry of NO. McLarnon and Penetrante found that charged species do not directly contribute to NO_x formation[45]. For example, electronically excited nitrogen molecules, such as the metastable $N_2(A)$ state, were found not to contribute directly to NO_x formation, but they can play an important role in O_2 dissociation via the reaction:

$$N_2(A) + O_2 \leftrightarrow N_2 + O + O \tag{22}$$
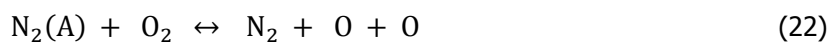
At higher oxygen concentrations, however, $N_2(A)$ densities will be low due to efficient quenching of this state on O_2.

The atomic N radical in reaction (19) can be electronically excited to $N(^2D)$, which has a higher rate than reaction (19) for gas temperatures below 3000 K[39].

$$N(^2D) \ + \ O_2 \ \leftrightarrow \ NO + O, \tag{23}$$

The dominant dissociation mechanism of N_2, other than reaction (18), is through dissociative recombination:

$$N_2^+ + \ e \ \leftrightarrow \ N + N, \tag{24}$$

which is reported to yield $N(^2D)$ and $N(^4S)$ in at least equal amounts[46,47], but has a significant energy cost due to the ionization energy of N_2 being lost with each reaction. The reverse of reaction (18) and reaction (20) show why the energy efficiency declines as the NO_x concentration increases; if there is more NO_x already in the active reactor volume, more atomic N and NO/NO_2 is lost to these reactions and more of the input power goes to heat. This is why there is an optimum in the 'contact time' between arcs and gas stream: too short and the optimum NO concentration is not reached, too long and power is wasted on reverse reactions.

Conclusions

This study has presented plasma assisted production of nitrogen oxides from air at atmospheric pressure in a milli-scale gliding arc reactor. We demonstrated through this study that commercially valuable chemicals, such as nitrogen oxides, can be produced in high concentrations by using only air as feed mixture in a non-thermal gliding arc reactor. This study clearly establishes the effect of oxygen percentage and various feed mixtures on NO_x production. Use of air (or air+O_2) instead of N_2+O_2 brings benefits from an operational and capital cost point-of-view for a containerized plant.

The O_2% in the feed is the critical parameter to produce higher concentrations of NO_x. A higher percentage of oxygen in the feed will produce more NO_2 than NO. Diluting feed mixtures with argon and preheating of the feed mixture has a negative effect on the amount of nitrogen oxide produced for approximately equal power input. Visualizing propagation of gliding arc via high speed imaging gives insight into gliding arc dynamics. It is shown that a lower flowrate facilitates significantly longer exposure of the process gas to gliding arcs. Lower flowrates (and correspondingly higher specific energy inputs) are not necessarily beneficial to gain higher energy efficiency, however, but do increase the amount of NO_x produced.

Also, the energy consumption by the benchmark, the industrial Haber-Bosch process, is reported to be 0.48 MJ/mol[10], while 4.8 MJ/mol is the optimum value achieved in this study. Therefore, application of milli-scale gliding arc reactors on an industrial scale is possible only when the energy consumption is decreased by a factor of 10 to reach the benchmark value. A possible route towards decreasing the energy consumption for NO formation is operating the reactor at reduced pressures (e.g. 500 mbar). The reduced collision frequency at reduced pressure would allow for greater non-equilibrium between gas temperature and vibrational temperature, thus further promoting the Zeldovich reaction chain[43]. Another possibility is the 'rotating gliding arc', where enhanced mixing of the gas is achieved compared to the linear gliding arc employed here, with possible benefits to the maximum achievable NOx concentration and the subsequent energy efficiency[48]. Employing gliding arc in decentralized, small scale fertilizer production plants using sustainable energy sources places lower restrictions on its application, however. Where the inherently intermittent supply of electricity from renewable sources such as wind and solar can surpasses the instantaneous demand, gliding arc in air can provide a fast, switchable, low-footprint method for producing a valuable product. The concept of de-centralized production of chemicals is gradually gaining an acceptance in chemical industry, to which this study adds new insights for the development of a containerized plasma nitrogen fixation process.

Acknowledgment

Literature Cited

1. Cowling E, Galloway J, Furiness C, et al. Optimizing nitrogen management in food and energy production and environmental protection: summary statement from the Second International Nitrogen Conference. *Sci World J*. 2001;1(2):1-9. doi:10.1100/tsw.2001.481.

2. Galloway JN, Cowling EB. Reactive nitrogen and the world: 200 years of change. *Ambio*. 2002;31(2):64-71. doi:10.2307/4315217.

3. Schrock RR. Reduction of dinitrogen. *Proc Natl Acad Sci U S A*. 2006;103(46):17087. doi:10.1073/pnas.0603633103.

4. Rafiqul I, Weber C, Lehmann B, Voss A. Energy efficiency improvements in ammonia production - Perspectives and uncertainties. *Energy*. 2005;30(13):2487-2504. doi:10.1016/j.energy.2004.12.004.

5. Tanabe Y, Nishibayashi Y. Developing more sustainable processes for ammonia synthesis. *Coord Chem Rev*. 2013;257(17-18):2551-2564. doi:10.1016/j.ccr.2013.02.010.

6. International Energy Agency-IEA. *Technology Roadmap: Energy and GHG Reductions in the Chemical Industry via Catalytic Processes*.; 2013.

7. Patil BS, Wang Q, Hessel V, Lang J. Plasma Assisted Nitrogen Fixation Reactions. In: Stefanidis GD, Stankiewicz A, eds. *Alternative Energy Sources For Green Chemistry*. Cambridge, UK: Royal Society of Chemistry; 2016. doi:10.1039/9781782623632-00296.

8. Lan R, Irvine JTS, Tao S. Ammonia and related chemicals as potential indirect hydrogen storage materials. *Int J Hydrogen Energy*. 2012;37(2):1482-1494. doi:10.1016/j.ijhydene.2011.10.004.

9. Lang J, Kling R, Brachhold H, Muller R, Pross G. Plasma Reactions. In: *Ullmann's Encyclopedia of Industrial Chemistry*. ; 2015:1-22.

10. Cherkasov N, Ibhadon AO, Fitzpatrick P. A review of the existing and alternative methods for greener nitrogen fixation. *Chem Eng Process Process Intensif*. 2015;90:24-33.

doi:10.1016/j.cep.2015.02.004.

11.   Patil BS, Wang Q, Hessel V, Lang J. Plasma N2-fixation: 1900–2014. *Catal Today*. 2015;256:49-66. doi:10.1016/j.cattod.2015.05.005.

12.   Hessel V, Cravotto G, Fitzpatrick P, Patil BS, Lang J, Bonrath W. Industrial applications of plasma , microwave and ultrasound techniques : Nitrogen-fixation and hydrogenation reactions. *Chem Eng Process Process Intensif*. 2013;71:19-30. doi:10.1016/j.cep.2013.02.002.

13.   Fridman A. *Plasma Chemistry*. New York: Cambridge University Press; 2008.

14.   Liberman MA, Lichtenberg AJ. *Principles of Plasma Discharges and Materials Processing*.; 2005.

15.   Samukawa S, Hori M, Rauf S, et al. The 2012 Plasma Roadmap. *J Phys D Appl Phys*. 2012;45(25):253001. doi:10.1088/0022-3727/45/25/253001.

16.   Patil BS, Cherkasov N, Lang J, Ibhadon AO, Hessel V, Wang Q. Low temperature plasma-catalytic NOx synthesis in a packed DBD reactor: Effect of support materials and supported active metal oxides. *Appl Catal B Environ*. 2016;194:123-133. doi:10.1016/j.apcatb.2016.04.055.

17.   Anastasopoulou A, Butala S, Lang J, Hessel V, Wang Q. Life Cycle Assessment of the Nitrogen Fixation Process Assisted by Plasma Technology and Incorporating Renewable Energy. *Ind Eng Chem Res*. 2016;55(29):8141-8153. doi:10.1021/acs.iecr.6b00145.

18.   Ingels R, Graves D, Anderson S, Koller R. Modern Plasma Technology for Nitrogen Fixation: New Opportunities? In: *International Fertiliser Society*. London, UK: International Fertiliser Society; 2015:1-27. http://fertiliser-society.org/proceedings/uk/Prc771.HTM.

19.   Fridman A, Nester S, Kennedy LA, Saveliev A, Mutaf-yardimci O. Gliding arc gas discharge. 1999;25:211-231.

20.   Czemichowski A. Gliding arc. Applications to engineering and environment control. 1994;66(6):1301-1310.

21.   Kolev S, Bogaerts a. A 2D model for a gliding arc discharge. *Plasma Sources Sci Technol*. 2015;24(1):15025. doi:10.1088/0963-0252/24/1/015025.

22.   Patil BS. Plasma (Catalyst) – Assisted Nitrogen Fixation : Reactor Development for Nitric Oxide and Ammonia Production. 2017.

23.   Indarto A, Yang DR, Choi JW, Lee H, Song HK. Gliding arc plasma processing of CO2 conversion. *J Hazard Mater*. 2007;146:309-315. doi:10.1016/j.jhazmat.2006.12.023.

24.   Pornmai K, Jindanin A, Sekiguchi H. Synthesis Gas Production from CO2 -Containing Natural Gas by Combined Steam Reforming and Partial Oxidation in an AC Gliding Arc Discharge. 2012:2-12. doi:10.1007/s11090-012-9371-2.

25.   Spasova B, Tiemann D, O'Connell M, Ziogas A, Kolb G, Hessel V. Synthesis gas production from methane and propane in a miniaturized GlidArc® reformer. *Int J Hydrogen Energy*. 2014;39(24):12657-12666. doi:10.1016/j.ijhydene.2014.06.065.

26.   Tu X, Whitehead JC. Plasma dry reforming of methane in an atmospheric pressure AC gliding arc discharge: Co-generation of syngas and carbon nanomaterials. *Int J Hydrogen Energy*. 2014;39(18):9658-9669. doi:10.1016/j.ijhydene.2014.04.073.

27.   Krawczyk K, Ulejczyk B. Decomposition of Chloromethanes in Gliding Discharges. *Plasma Chem Plasma Process*. 2003;23(2):265-281. doi:10.1023/A:1022916018245.

28.   Dalaine V, Cormier JM, Lefaucheux P. A gliding discharge applied to H2S destruction. *J Appl Phys*. 1998;83(5):2435-2441. doi:10.1002/chem.201304722.

29.   Krawczyk K, Mlotek M. Combined plasma-catalytic processing of nitrous oxide. *Appl Catal B Environ*. 2001;30(3-4):233-245. doi:10.1016/S0926-3373(00)00243-5.

30.   Thiemann M, Scheibler E, Wiegand KW. Nitric Acid, Nitrous Acid, and Nitrogen Oxides. In: *Ullmann's Encyclopedia of Industrial Chemistry*. Wiley-VCH Verlag GmbH & Co. KGaA; 2000. doi:10.1002/14356007.a17_293.

31.   Burlica R, Kirkpatrick MJ, Locke BR. Formation of reactive species in gliding arc discharges with liquid water. *J Electrostat*. 2006;64(1):35-43. doi:10.1016/j.elstat.2004.12.007.

32.   Cormier JM, Aubry O, Khacef A. Degradation of organics compounds and production of activated

species in dielectric barrier discharges and glidarc reactors. *NATO Secur through Sci Ser A Chem Biol.* 2008:125-134. doi:10.1007/978-1-4020-8439-3_10.

33.   Czekalska Z. Gases Conversion in Low Temperature Plasma. *Arch Combust.* 2010;30(4):337-346.

34.   Bo Z, Yan J, Li X, Chi Y, Cen K. Nitrogen dioxide formation in the gliding arc discharge-assisted decomposition of volatile organic compounds. *J Hazard Mater.* 2009;166(2-3):1210-1216. doi:10.1016/j.jhazmat.2008.12.030.

35.   Patil BS, Rovira Palau J, Hessel V, Lang J, Wang Q. Plasma Nitrogen Oxides Synthesis in a Milli-Scale Gliding Arc Reactor: Investigating the Electrical and Process Prameters. *Plasma Chemsiry Plasma Process.* 2016;36:241-257. doi:10.1007/s11090-015-9671-4.

36.   Yang J, Li T, Zhong C, Guan X, Hu C. Nitrogen Fixation in Water Using Air Phase Gliding Arc Plasma. *J Electrochem Soc.* 2016;163(10):E288-E292. doi:10.1149/2.0221610jes.

37.   Rueangjitt N, Sreethawong T, Chavadej S, Sekiguchi H. Plasma-catalytic reforming of methane in AC microsized gliding arc discharge: Effects of input power, reactor thickness, and catalyst existence. *Chem Eng J.* 2009;155(3):874-880. doi:10.1016/j.cej.2009.10.009.

38.   Hong J, Prawer S, Murphy AB. Production of Ammonia by Heterogeneous Catalysis in a Packed-Bed Dielectric-Barrier Discharge : Influence of Argon Addition and Voltage. *IEEE Trans PLASMA Sci.* 2014;42(10):2338-2339.

39.   Sakiyama Y, Graves DB, Chang H-W, Shimizu T, Morfill GE. Plasma chemistry model of surface microdischarge in humid air and dynamics of reactive neutral species. *J Phys D Appl Phys.* 2012;45(42):425201. doi:10.1088/0022-3727/45/42/425201.

40.   Ammann PR, Timmins RS. Chemical Reactions During Rapid Quenching of Oxygen-Nitrogen Mixtures from Very High Temperatures. *AIChE J.* 1966;12(5):956-963.

41.   Sun ZW, Zhu JJ, Li ZS, et al. Optical diagnostics of a gliding arc. *Opt Express.* 2013;21(5):6028-6044. doi:10.1364/OE.21.006028.

42.   Tu X, Gallon HJ, Whitehead JC. Dynamic behavior of an atmospheric argon gliding arc plasma.

IEEE Trans Plasma Sci. 2011;39(11 PART 1):2900-2901. doi:10.1109/TPS.2011.2150247.

43.   Wang W, Patil BS, Heijkers S, Hessel V, Bogaerts A. Nitrogen fixation by gliding arc plasma: Better insight by chemical kinetics modeling. *ChemSusChem*. 2017;10:2145-2157. doi:10.1002/cssc.201700095.

44.   Indarto A, Choi JW, Lee H, Song HK. Effect of additive gases on methane conversion using gliding arc discharge. *Energy*. 2006;31(14):2650-2659. doi:10.1016/j.energy.2005.10.034.

45.   Herron JT. Modeling Studies of the Formation and Destruction of NO in Pulsed Barrier Discharges in Nitrogen and Air. *Plasma Chem Plasma Process*. 2001;21(4):581-609.

46.   Cosby PC. Electron-impact dissociation of nitrogen. *J Chem Phys*. 1993;98(12):9544. doi:10.1063/1.464385.

47.   Hill RD, Rahmim I, Rinker RG. Experimental Study of the Production of NO, N20, and O3 in a Simulated Atmospheric Corona. *Ind Eng Chem Res*. 1988;27(7):1264-1269.

48.   ZHANG H, ZHU F, LI X, DU C. Dynamic behavior of a rotating gliding arc plasma in nitrogen: effects of gas flow rate and operating current. *Plasma Sci Technol*. 2017;19(4):45401. doi:10.1088/2058-6272/aa57f3.
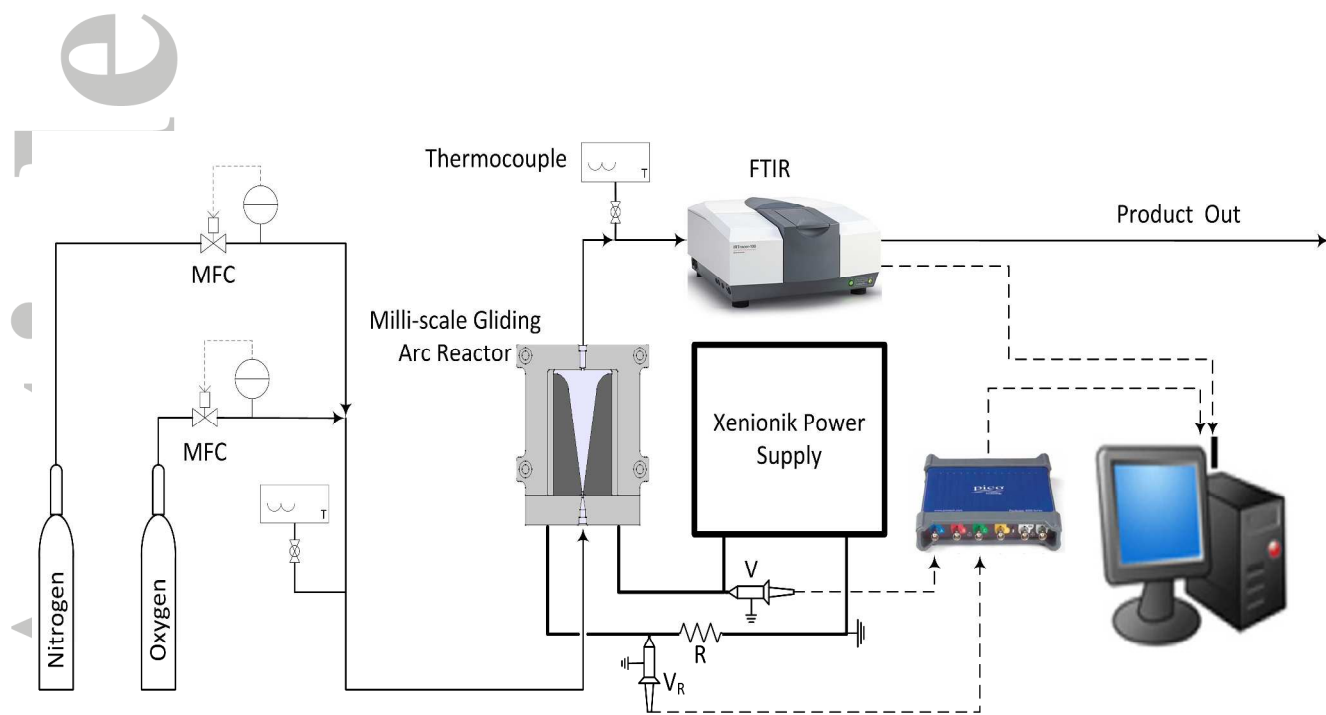
List of Figure captions

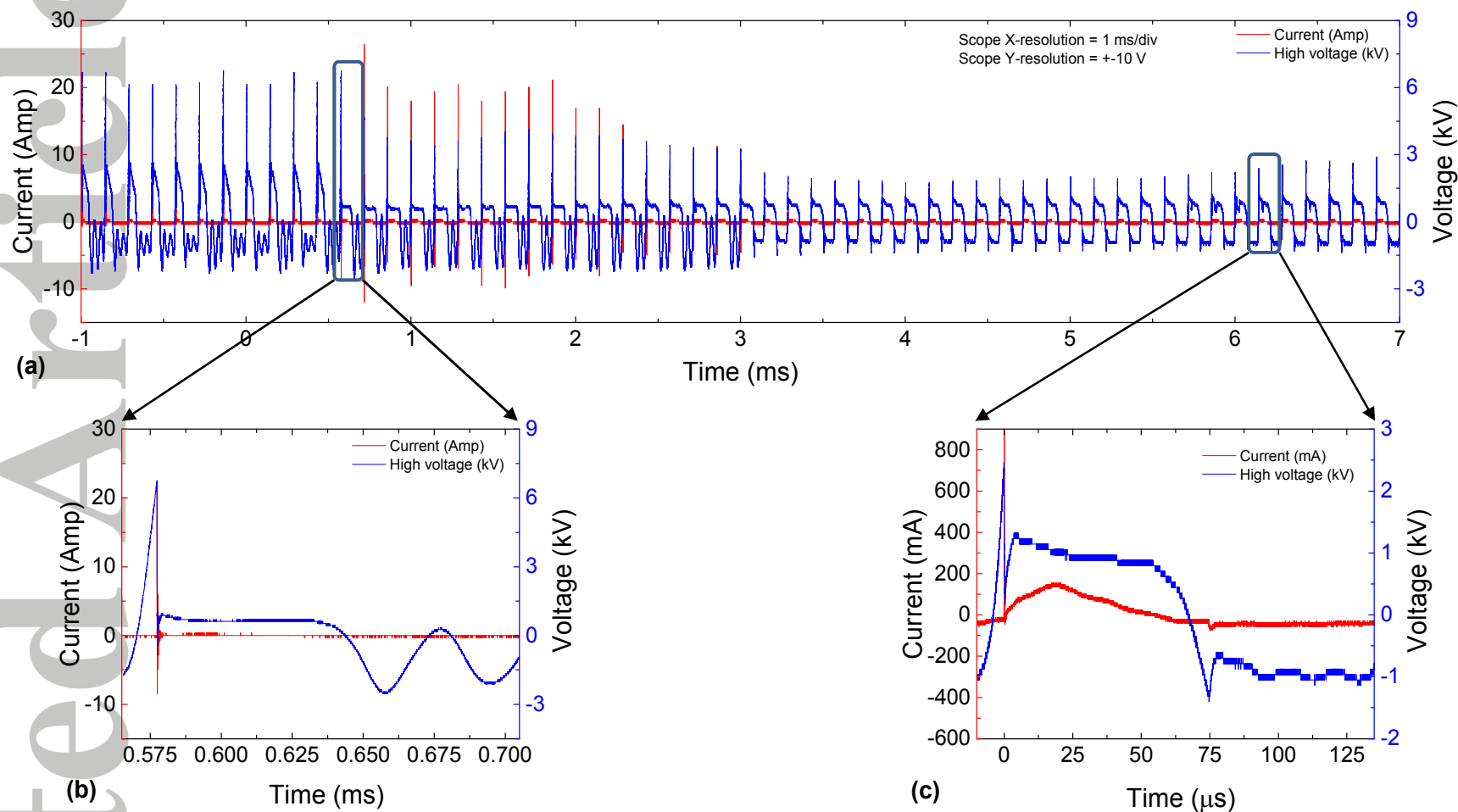**Figure 1. Schematic of the milli-scale gliding arc and the experimental set-up.**

Figure 2. Voltage-current signal for the milli-scale gliding arc reactor with different scope resolutions (a) A complete gliding arc cycle of ~8 ms duration (b) Ignition of arc with currents up to ~25 A, (c) Propagation of arc with current < 1 A (at 7 kHz-25 μs, 0.5 L/min of Air+O_2 with N_2/O_2 ratio=1 and waveform generator input voltage 60 V_{pk-pk}).
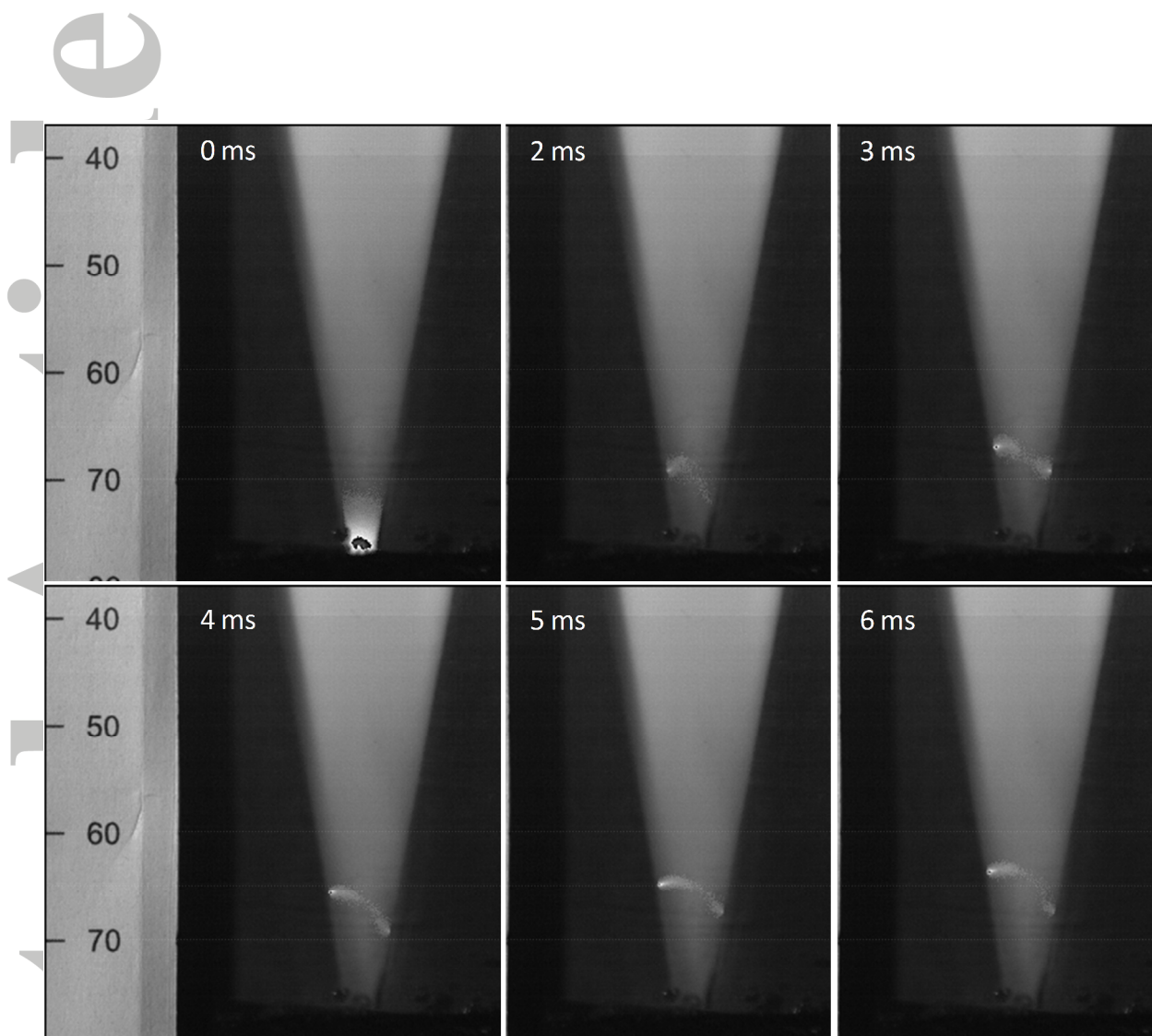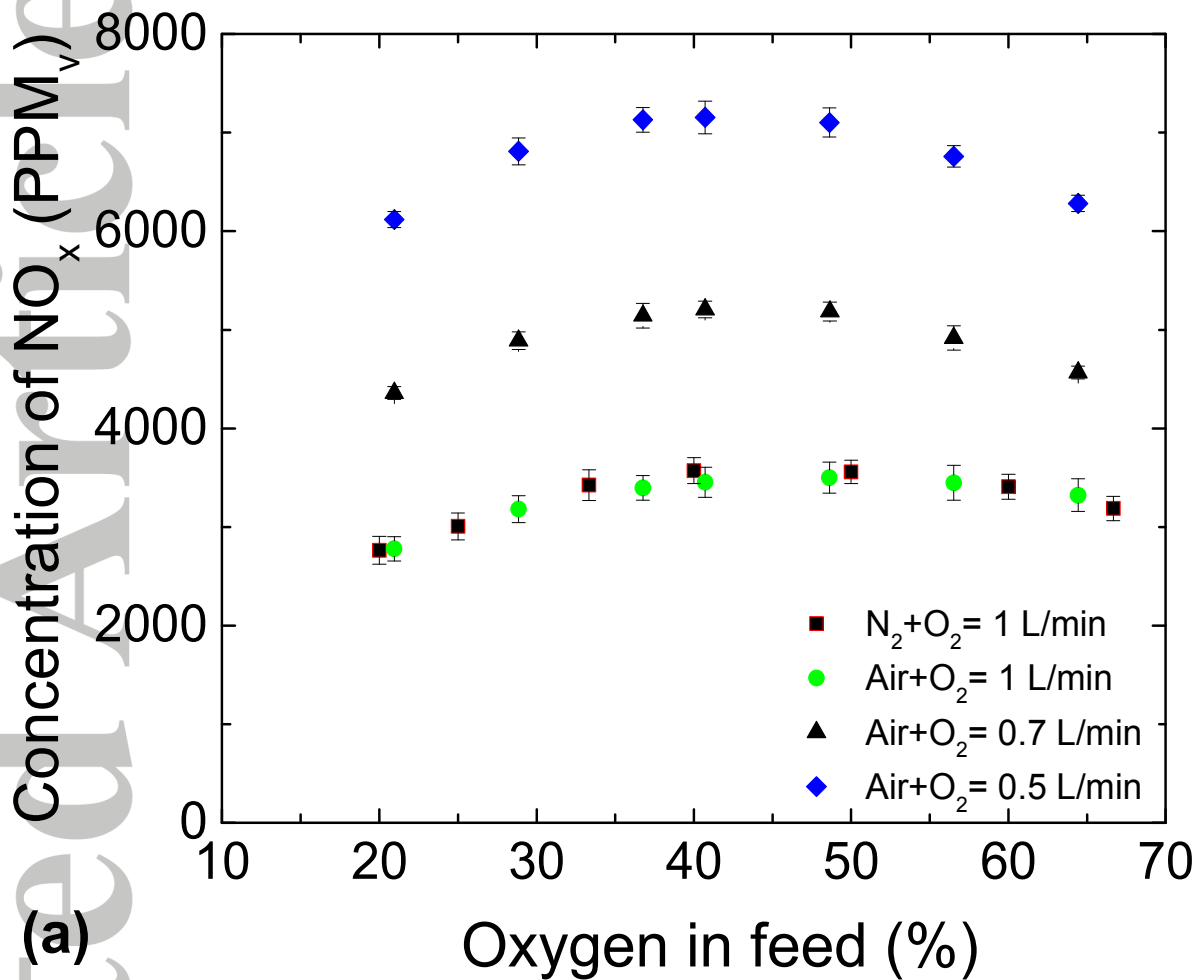
Figure 3. Visualization of the gliding arc propagation along the reactor as a function of time by means of high speed recordings for the inlet feed flow rate = 1 L/min; N_2/O_2 = 1. Frame rate = 3 kHz with resolution of 512 X 512.
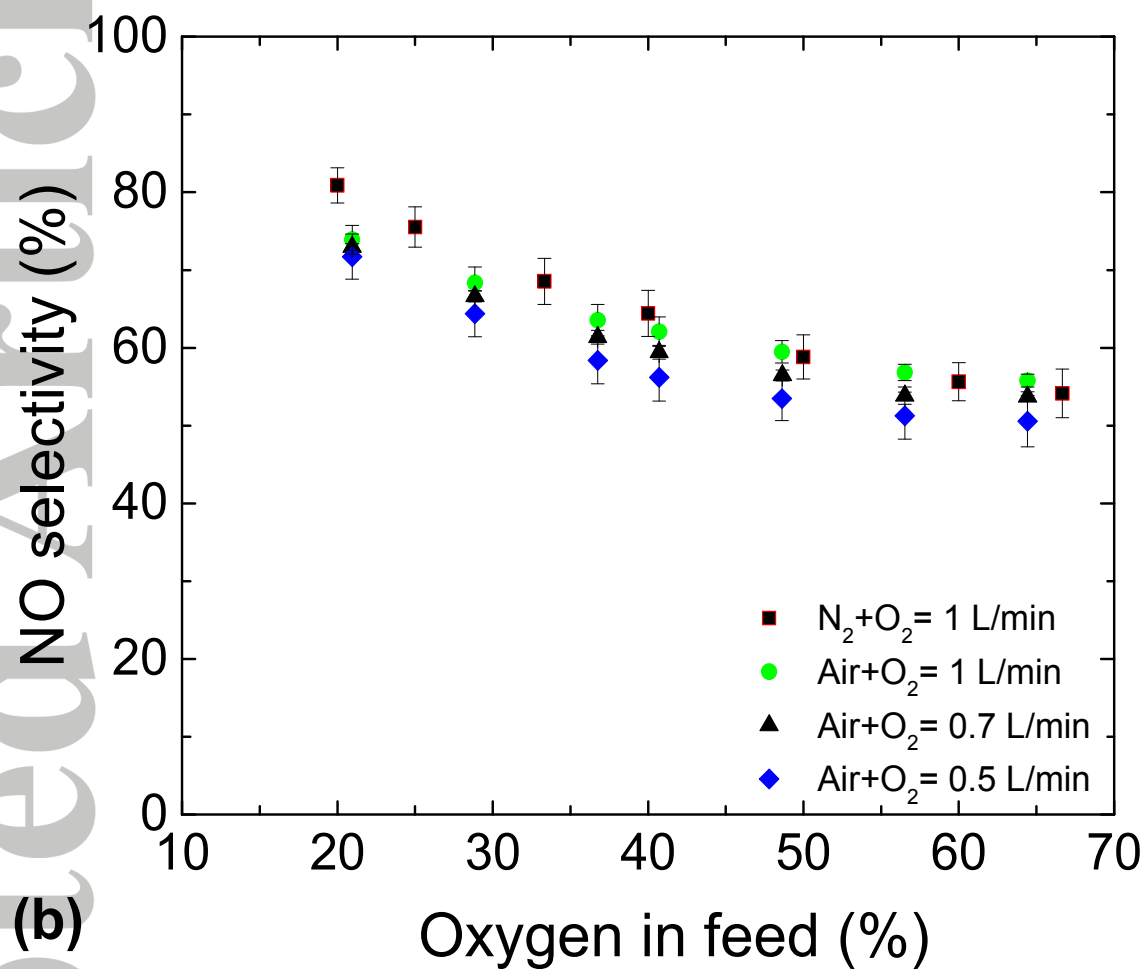
Figure 4. Effect of different feeds and N_2/O_2 ratio on- a. NOx concentration and b. NO selectivity (frequency= 7 kHz, input power ~ 12 W with SEI between $700 - 1500$ J/L).
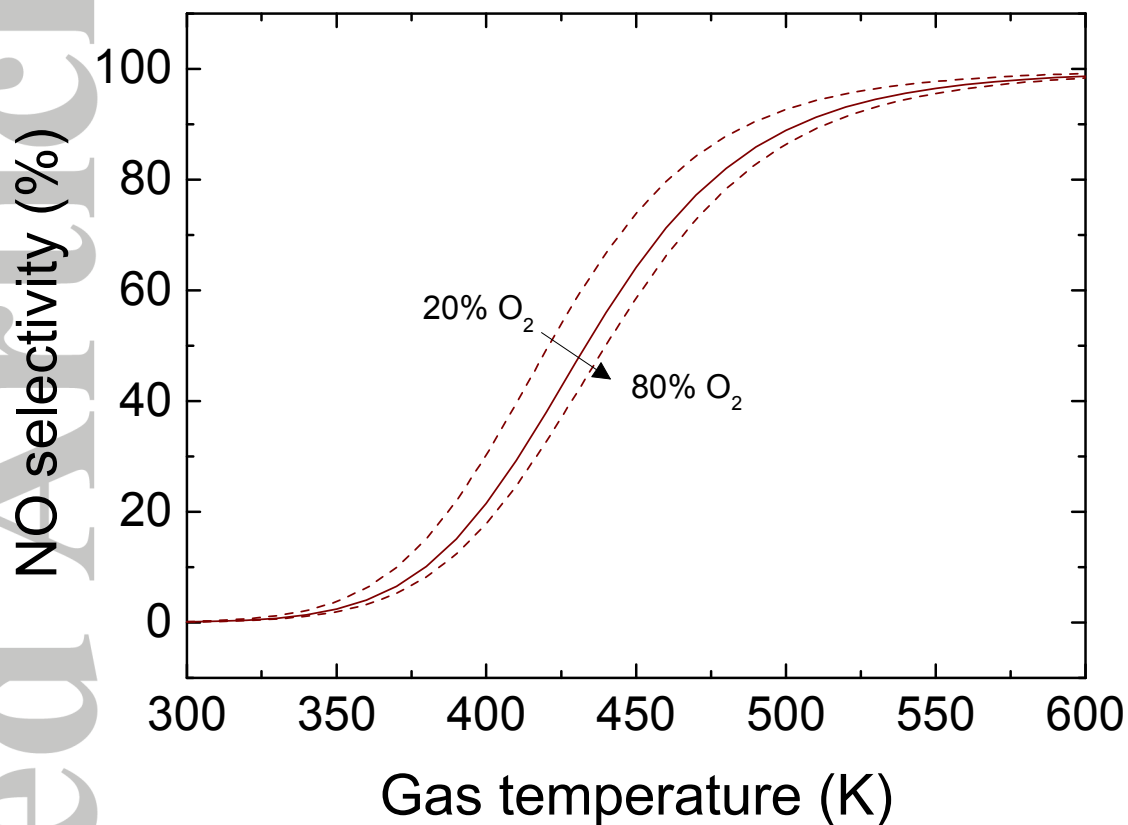
Figure 5. NO selectivity at equilibrium for different oxygen content as a function of gas temperature. The solid line is for 50% O_2 content and the dashed lines for 20% and 80%.
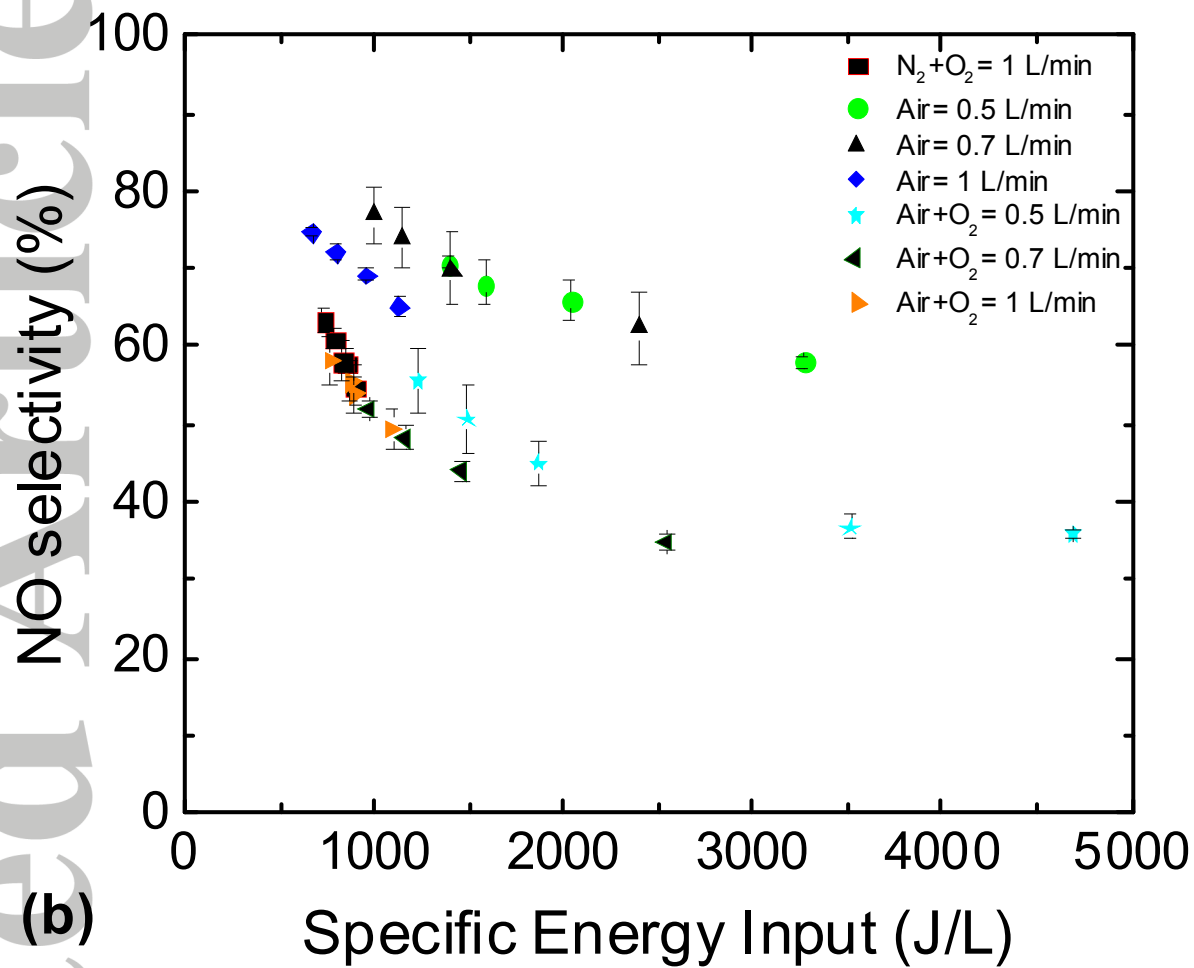
Figure 6. Effect of flowrate on- a. NO_x concentration and b. NO selectivity (at frequency= 7 kHz, input power between $12 - 40$ W).

Figure 7. Effect of Ar addition on- a. NO_x concentration and b. NO selectivity (at frequency= 7 kHz, power input ~ 12 - 10 W).

Figure 8. Feed gas preheating has negative impact on NO_x concentration (at frequency= 7 kHz, input power between 12 W plasma + 0 W electric heating (lowest temperature) and 10 W + 5 W electric heating (highest temperature)).

Figure 9. Energy efficiency of Plasma NO_x synthesis- a. for different O_2 % in feed and b. for different flowrates. (Plasma power between $12 - 44$ W).

Figure 1. Schematic of the milli-scale gliding arc and the experimental set-up.

Figure 2. Voltage-current signal for the milli-scale gliding arc reactor with different scope resolutions (a) A complete gliding arc cycle of ~8 ms duration (b) Ignition of arc with currents up to ~25 A, (c) Propagation of arc with current < 1 A (at 7 kHz-25 μs, 0.5 L/min of Air+O_2 with N_2/O_2 ratio=1 and waveform generator input voltage 60 V_{pk-pk}).

Figure 3. Visualization of the gliding arc propagation along the reactor as a function of time by means of high speed recordings for the inlet feed flow rate = 1 L/min; N_2/O_2 = 1. Frame rate = 3 kHz with resolution of 512X512.

(a)

(b)

Figure 4. Effect of different feeds and N_2/O_2 ratio on- a. NOx concentration and b. NO selectivity

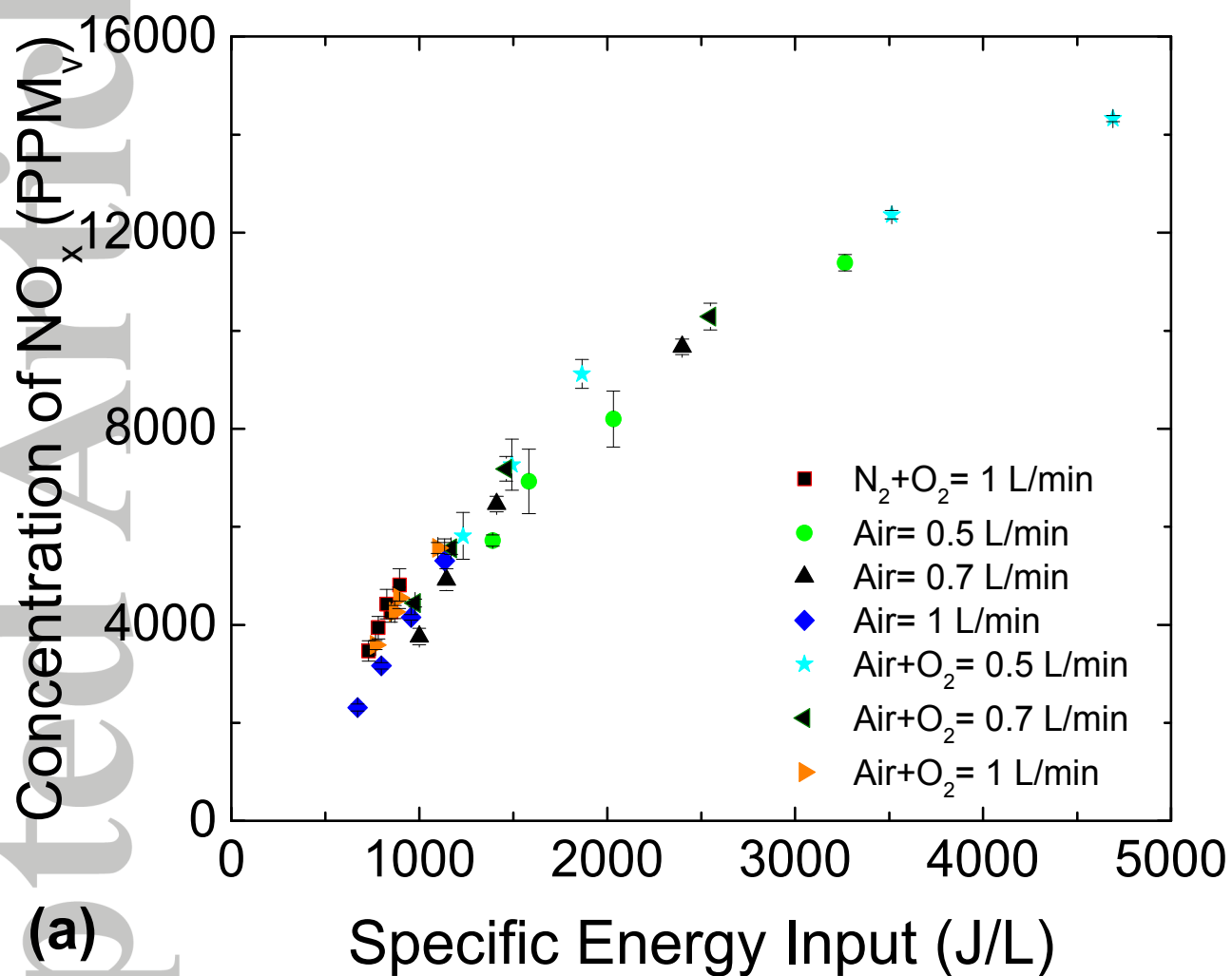(frequency= 7 kHz, input power ~ 12 W with SEI between $700 - 1500$ J/L).

Figure 5. NO selectivity at equilibrium for different oxygen content as a function of gas temperature. The solid line is for 50% O$_2$ content and the dashed lines for 20% and 80%.
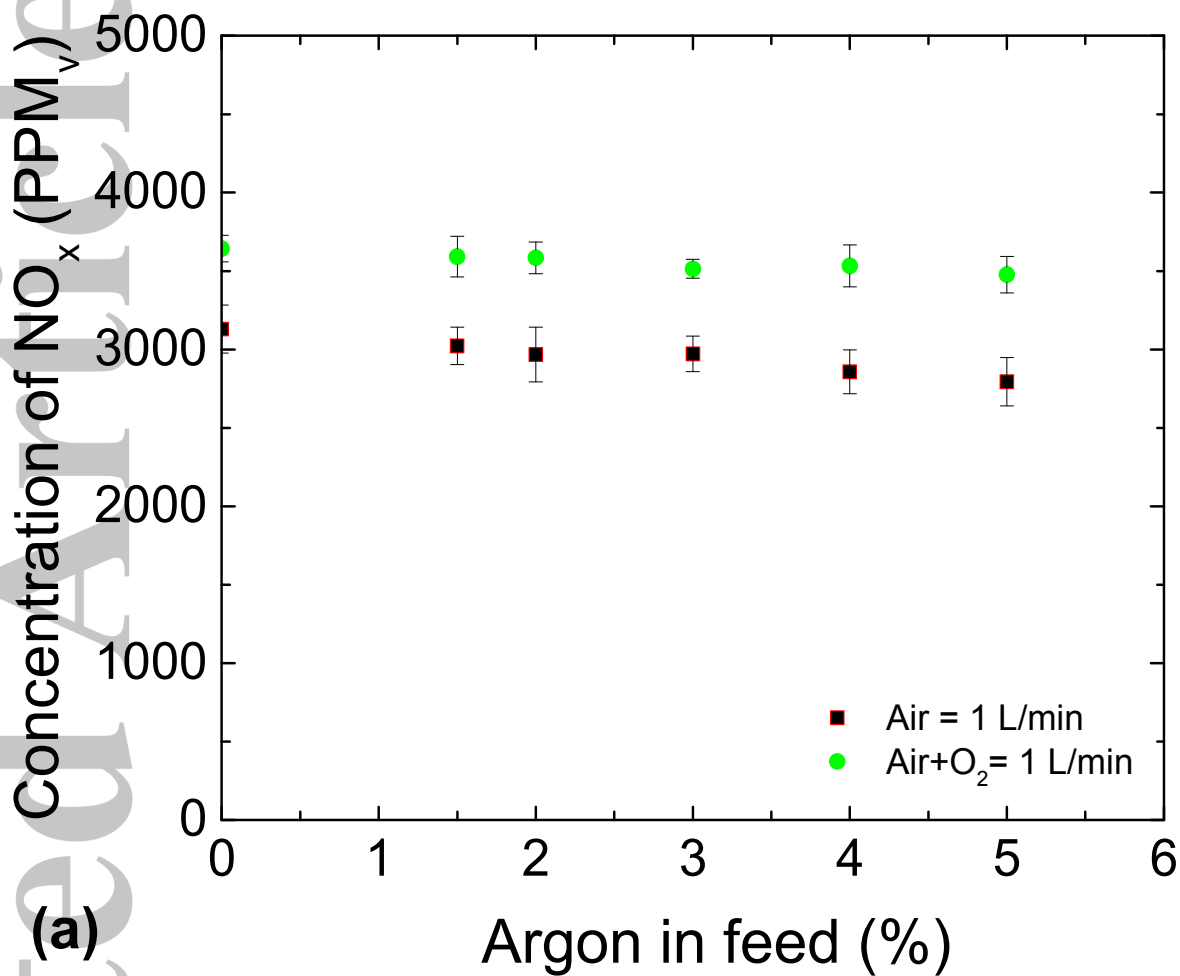
(a)

Legend:
- $N_2+O_2= 1$ L/min
- Air= 0.5 L/min
- Air= 0.7 L/min
- Air= 1 L/min
- Air+O_2= 0.5 L/min
- Air+O_2= 0.7 L/min
- Air+O_2= 1 L/min

Y-axis: Concentration of NO_x (PPM$_v$)

X-axis: Specific Energy Input (J/L)

Figure 6. Effect of flowrate on- a. NO$_x$ concentration and b. NO selectivity (at frequency= 7 kHz, input power between 12 − 40 W).

(a)

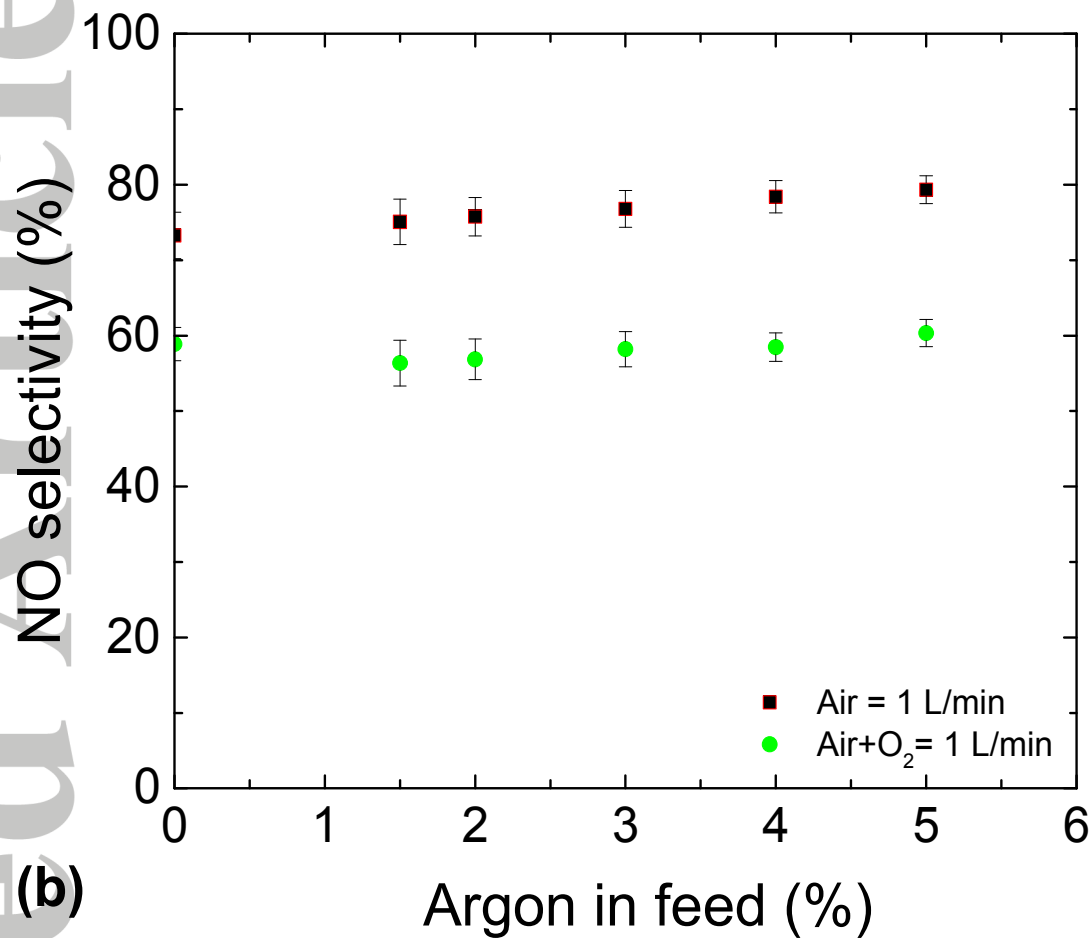**Figure 7. Effect of Ar addition on- a. NO$_x$ concentration and b. NO selectivity (at frequency= 7 kHz, power input ~ 12 - 10 W).**
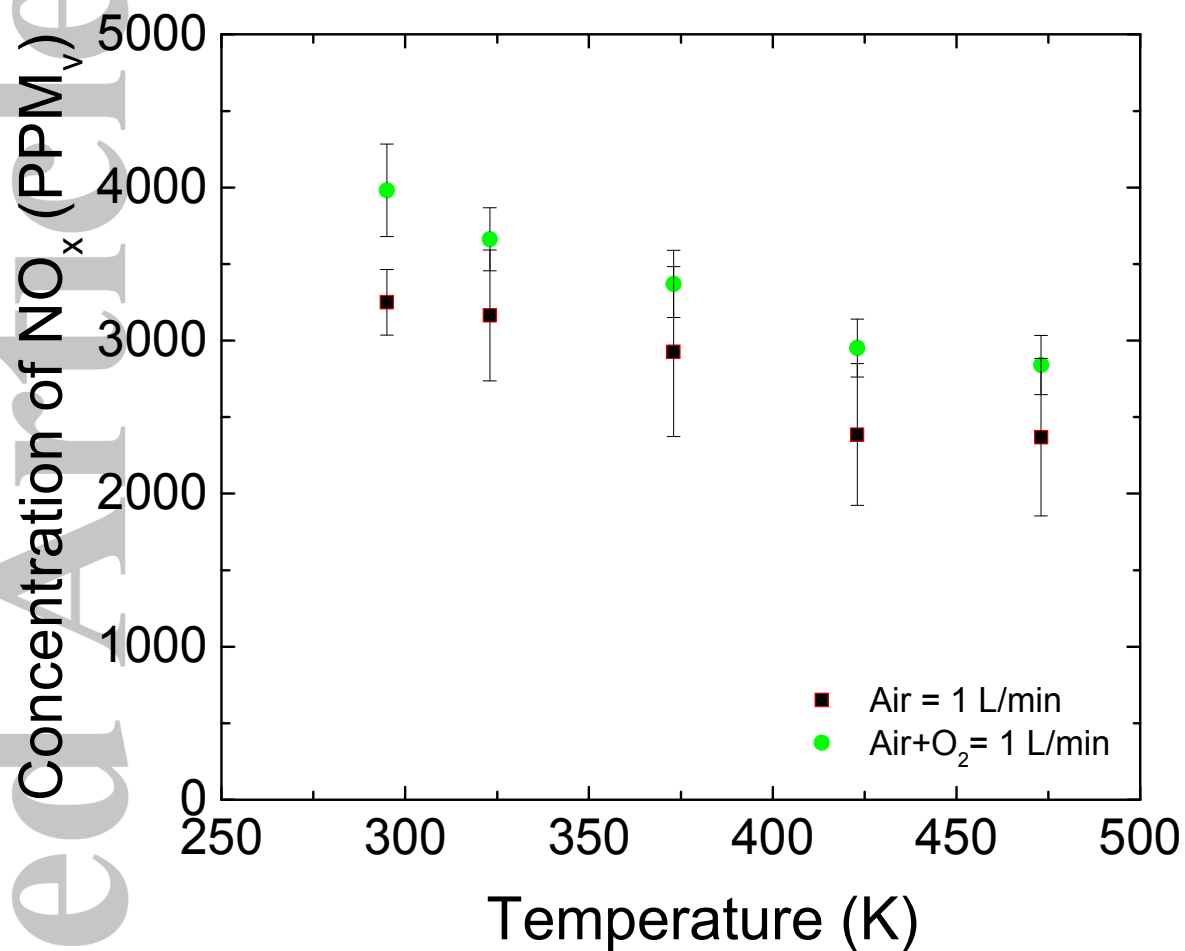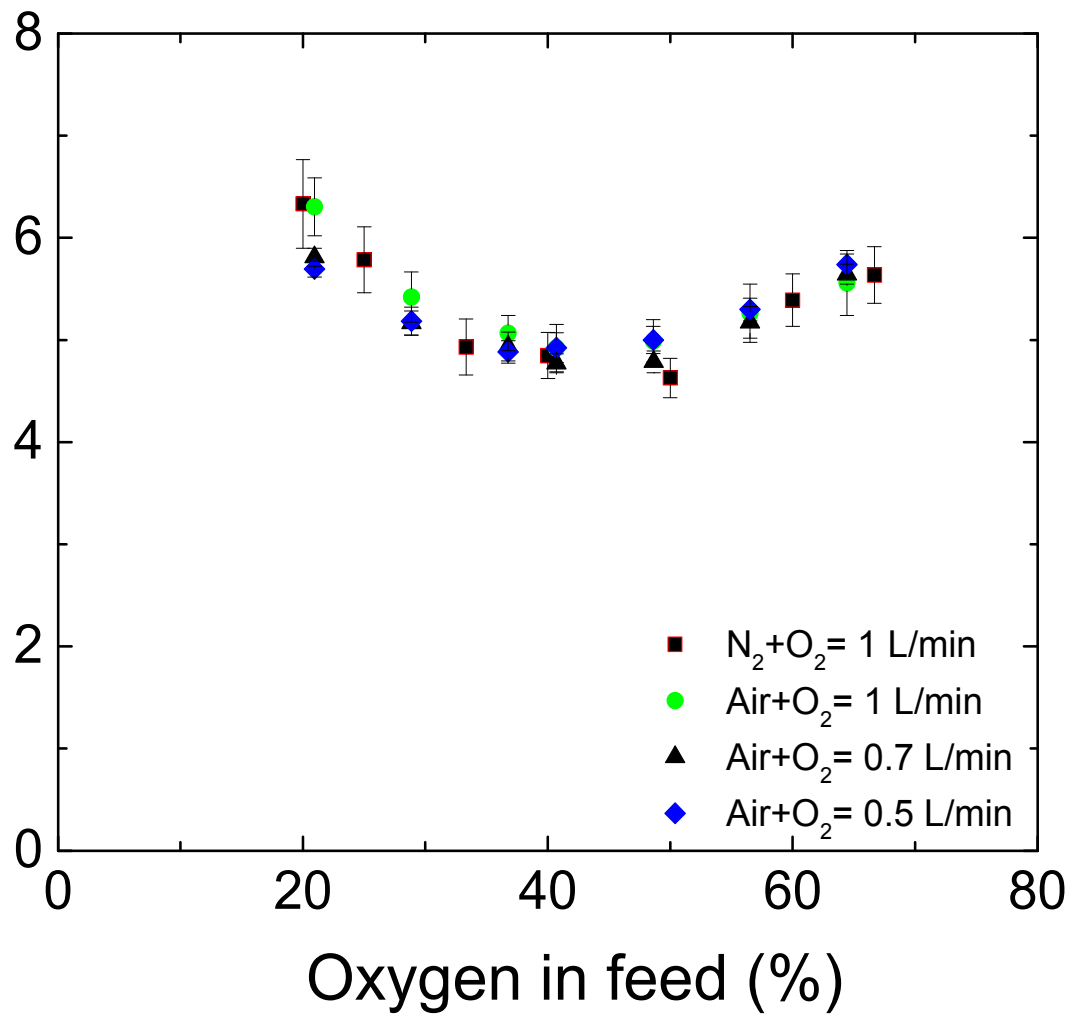
Figure 8. Feed gas preheating has negative impact on NO$_x$ concentration (at frequency= 7 kHz, input power between 12 W plasma + 0 W electric heating (lowest temperature) and 10 W + 5 W electric heating (highest temperature)).
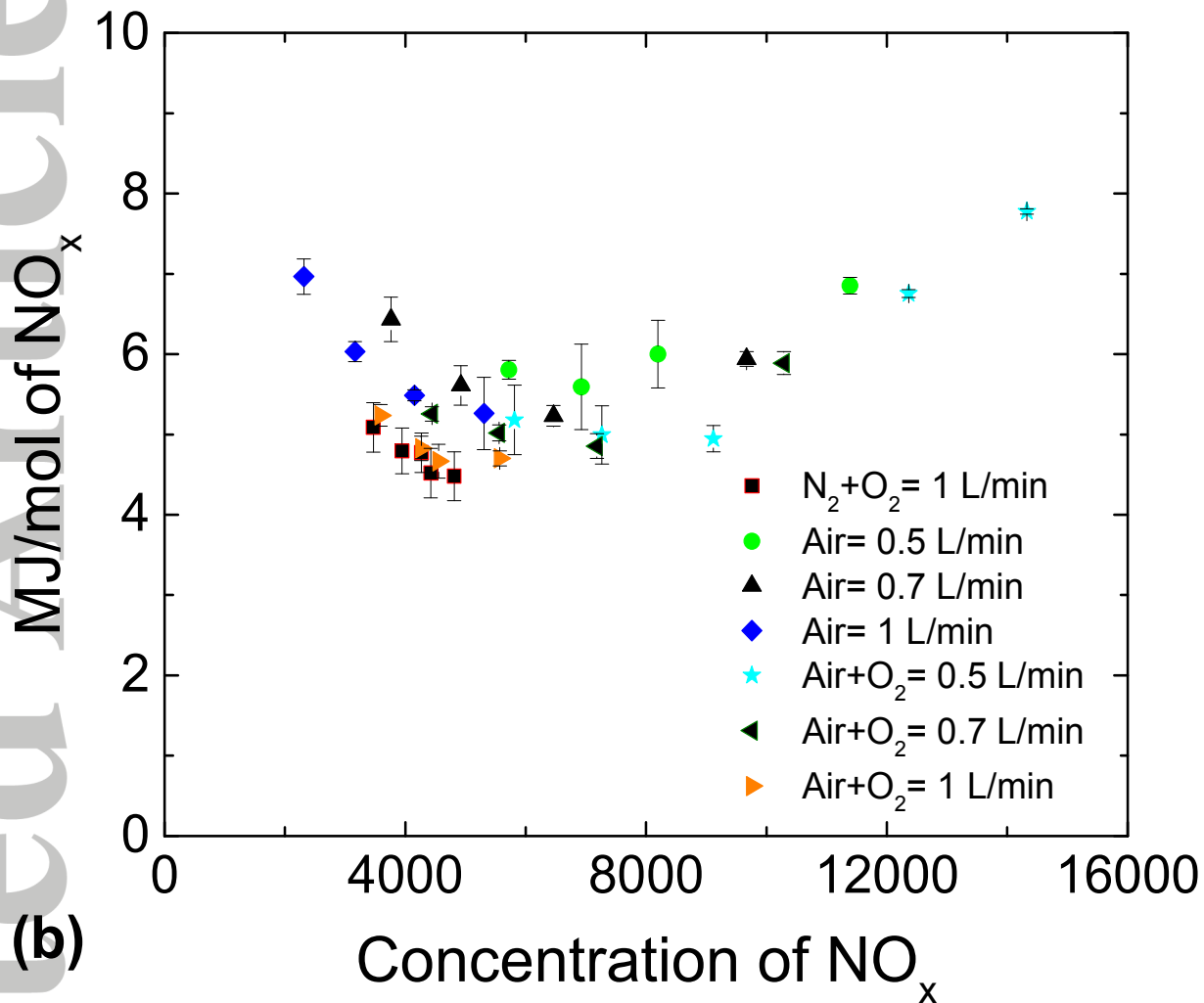
(a)

(b)

Figure 9. Energy efficiency of Plasma NO_x synthesis- a. for different O_2 % in feed and b. for different

flowrates. (Plasma power between 12 – 44 W).

Table 1. Summary of the Results obtained by High-Speed Imaging

Feed and flow rate (L/min)	Average gliding arc height (mm)	Average gliding arc propagation time (ms)	Average gliding arc velocity (m/s)	Average gas flow velocity (m/s)
Air = 0.5	10.3	14.5	0.71	0.87
Air = 0.7	7.54	8.2	0.92	1.40
Air = 1	6.93	4.2	1.65	2.10
$N_2+O_2 = 1$ ($N_2/O_2=1$)	9.7	6.6	1.47	1.80

Table 2. Rates for Production and Destruction of Higher Nitrogen Oxides at 450 K[39]

Reaction number	$k_{forward}$ $(m^6 s^{-1})$ or *$(m^3 s^{-1})$	$k_{backward}$ $(m^3 s^{-1})$	Species	Estimated concentration of NO_3 and N_2O_x (ppb)
12	$6.01 \cdot 10^{-59}$	$2.61 \cdot 10^{-40}$		
			NO_3	<< 1
13	$6.33 \cdot 10^{-29*}$	$5.14 \cdot 10^{-17}$		
14	$1.36 \cdot 10^{-47}$	$3.00 \cdot 10^{-19}$	N_2O_3	8.8
15	$2.51 \cdot 10^{-46}$	$1.81 \cdot 10^{-18}$	N_2O_4	20
16	$6.77 \cdot 10^{-42}$	$5.86 \cdot 10^{-21}$	N_2O_5	<< 1